Effective base isolation combining low-friction curved surface sliders and hysteretic gap dampers

Dario De Domenico [1*], Emanuele Gandelli [2], Virginio Quaglini [2]

[1] Department of Engineering, University of Messina, Contrada Di Dio, 98166 Sant'Agata, Messina, Italy
[2] Department of Architecture, Built Environment and Construction Engineering, Politecnico di Milano, Piazza Leonardo da Vinci 31, 20133 Milano, Italy

* Corresponding author: Dario De Domenico, University of Messina. Email: dario.dedomenico@unime.it

ABSTRACT

The re-centering capability represents a fundamental property of any effective isolation system. Indeed, a potential residual displacement after an earthquake, besides affecting the serviceability of the construction, may also result in increased peak displacements during aftershocks and future events. In curved surface sliders (CSSs), energy dissipation and re-centering capability are two competing aspects influenced by the friction coefficient and the state of lubrication of the sliding pad. On the one hand, the large energy dissipation capability of high-friction CSSs contributes to mitigate the displacement demand during strong events but negatively affects the re-centering behavior. On the other hand, low-friction CSSs exhibit a better re-centering behavior, but are expected to undergo large displacements that, in turn, imply large dimensions in plan and pose problems of possible pounding between adjacent buildings and damage of nonstructural elements, lifelines and utilities crossing the isolation joint. The present study proposes an efficient base-isolation system that combines low-friction CSSs with hysteretic gap dampers. The latter device introduces supplemental energy dissipation only when the displacement of the isolation system exceeds a threshold or initial gap while not being engaged otherwise. The mechanical properties of the gap damper are designed to provide a target energy dissipation such that the displacement demand of low-friction CSSs can be kept to the same level as that of high-friction CSSs. A parametric study comprising a series of nonlinear response history analyses and different CSS characteristics demonstrates that the supplemental dissipative mechanism of the gap damper does not impair the re-centering capability of the CSS isolators. These outcomes are additionally validated by comparing numerical simulations of a 3D base-isolated case-study frame with shake-table test results. The proposed base-isolation system efficiently combines satisfactory energy dissipation, which reduces the displacement demand, with high re-centering capability resulting in negligible residual displacements.

KEY WORDS: Base isolation; Curved surface slider; Displacement demand; Re-centering capability; Gap damper; Residual displacement; Friction coefficient.

1. INTRODUCTION

Base isolation is a well-established seismic protection strategy for buildings, bridges and industrial facilities, and its effectiveness has been widely demonstrated through analytical studies, shake-table tests as well as observations during real earthquakes [1]-[5]. This strategy is practically implemented by interposing low lateral stiffness devices between the construction and its foundations, in order to decouple the movement of the supported structure from the seismic motion of the ground. Among these devices, the most popular ones are the elastomeric bearings [6] and the sliding bearings with curved surfaces [7], originally introduced in North America under the trademark name of Friction Pendulum System (FPS), and known in Europe as Curved Surface Sliders (CSSs). Isolation devices provide some inherent (viscous, hysteretic or friction) damping. Thus, the isolation system lengthens the first-mode period of the structure while simultaneously increases the energy dissipation. This results in lower earthquake-induced forces and structural accelerations, while the seismic displacement is concentrated at the isolation level. The displacement demand may be huge, even of the order of 40-70 cm depending on the isolation period and the intensity of the ground motion, as reported in manufacturer's datasheets [8]-[10]. Large displacement demands entail the use of large-size isolators capable to accommodate the required displacements, and can be an issue for nonstructural elements, lifelines and in general for utilities crossing the joints between the isolated structure and the surrounding ground (i.e. elevators, waterworks, gas fittings and electrical conduits in buildings, road joints in bridges), which must accommodate the bearings' movements without failure. Additionally, in densely populated areas the risk of pounding between adjacent isolated buildings increases as a result of the large displacements of the isolators [11]. Therefore, the development of viable solutions aimed at reducing the displacement demand of the isolation system is of primary interest for both structural designers and manufacturers.

Different strategies to limit the seismic displacement of the isolation system have been proposed

so far in the literature. The isolation system can indeed be designed such that its stiffness increases at large displacements. In elastomeric bearings the large displacement stiffening may be achieved via strain-induced crystallization of the fillers [12], while in CSS this may be realized through an increase in the radius of curvature and/or the coefficient of friction of the external area of the sliding surface [13], [14]. Alternatively, hybrid control strategies combining the isolation system with a tuned mass damper (TMD) [15]-[17] or enhanced variants with an inerter [18]-[21], located above or below the isolation layer, have been proposed. Sliding hydromagnetic bearings and sliding implant-magnetic bearings also represent a promising solution providing adaptive energy dissipation and alterable deflection constraint, as recently shown in experimental tests [22] and numerical simulations [23], [24]. Another straightforward solution consists in providing supplemental damping in addition to the inherent damping of the isolators, e.g., by means of fluid viscous dampers, although this strategy was shown to increase the higher mode response and, consequently, to produce higher interstory drifts and floor accelerations in the superstructure [25].

Beside the displacement capacity d_{max}, another fundamental property of any effective isolation system is the re-centering capability, i.e. the ability of recovering the original position at the end of the earthquake [26]. A parameter used to quantify this capability is the residual displacement d_{res} after a seismic event [27]: such residual displacement results in a permanent offset of the isolation system, which not only can affect the serviceability of the structure, but may also produce an accrual of displacements in case of aftershocks and future events [28]. In CSSs, displacement demand, energy dissipation and re-centering capability are affected by the coefficient of friction of the sliding pad [29]-[31]. In particular, the displacement demand may be reduced by increasing damping through the use of high friction coefficients, but at the expense of a decreased re-centering capability. On the other hand, low friction coefficients are associated with a good re-centering behavior, but entail large displacements.

Since energy dissipation and re-centering capability of the CSS are two competing aspects, an

optimal isolation strategy can be developed based on the concept of introducing supplemental damping beyond a certain displacement, while keeping friction low in order not to impair re-centering of the isolation system as a whole. The concept is developed in this study, which proposes an effective base-isolation layout that combines low-friction CSSs with gap dampers [32]-[34]. The hysteretic properties of the gap damper are designed according to a performance-oriented design procedure, assuming a target displacement demand of the combined isolation system (low-friction CSS + gap damper) equivalent to the demand of high-friction CSSs under the maximum credible design earthquake. A parametric study, consisting of a series of nonlinear response history analyses for different CSS characteristics, demonstrates that the supplemental energy dissipation introduced by the gap damper does not impair the re-centering capability of the CSSs even during weak "serviceability" earthquakes. The outcomes are eventually confirmed by comparing numerical simulations of a 3D base-isolated case-study frame with shake-table test results.

Therefore, the proposed combined base isolation system is characterized by negligible residual displacement, as a result of the low friction coefficient of the CSSs, and reduced displacement demand, provided by the supplemental energy dissipation introduced by the gap damper.

2. THEORETICAL CONSIDERATIONS ON RE-CENTERING CAPABILITY OF CSS

The mechanical behavior of the CSS is conventionally described by a bilinear hysteretic model. The re-centering action is provided by the curved surface (with effective radius R_{eff}), while the energy dissipation is provided by the friction properties of the sliding pad. The friction coefficient generally ranges from 0.02 to 0.12 depending on the sliding material (commonly, PTFE or UHMWPE), the lubrication, the sliding velocity, the contact pressure and the temperature [35], [36]. Based on Figure 1, the horizontal reaction force of the CSS is the sum of the restoring force F_r due to the re-centering component and the frictional force F_f that is independent from the displacement

$$F = F_r + F_f = K_p\, d + F_0 \operatorname{sgn}\left(\dot{d}\right) \tag{1}$$

where $F_0 = \mu_d \cdot N$ represents the characteristic strength, which depends upon the dynamic coefficient of friction μ_d and the vertical load acting on the bearing N, $K_p = N / R_{\text{eff}}$ is the restoring stiffness, d denotes the horizontal displacement and $\text{sgn}\left(\dot{d}\right)$ the signum function of the horizontal velocity.

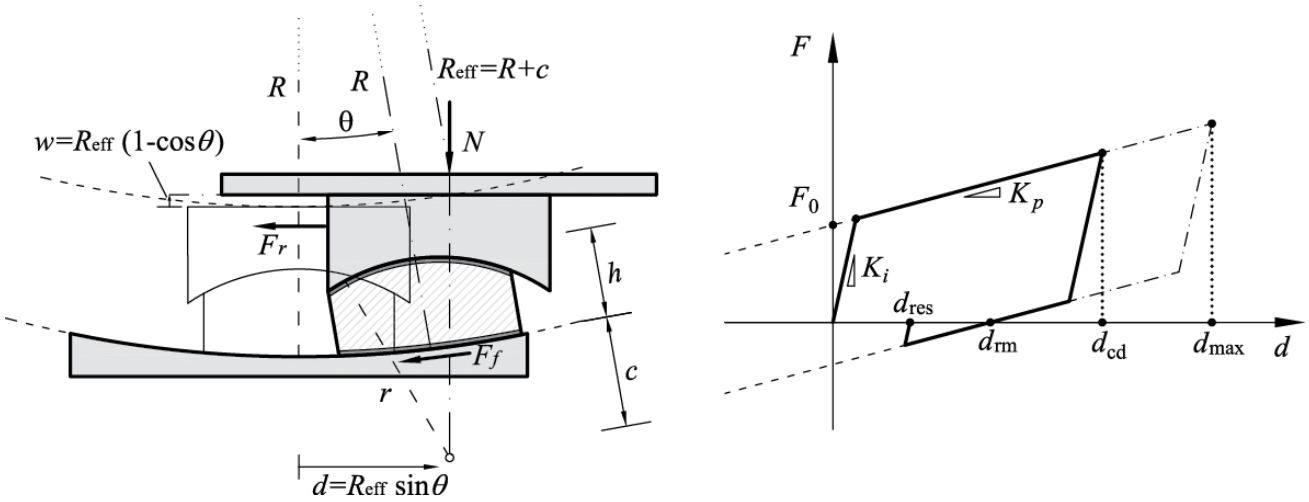

Figure 1 Kinematics of a single curved surface slider (left) and idealized bilinear hysteretic model (right)

The initial, or pre-sliding stiffness of the CSS is generally very high , e.g., $K_i \approx 50-100K_p$ [31], so that the yield displacement at which sliding starts is usually negligible. From Figure 1 it can be noted that the CSS can be in static equilibrium with zero resultant force when the restoring force $F_r = K_p \cdot d$, which always acts towards the origin, equilibrates the frictional force $F_f = \mu_d \cdot N$, whose direction is opposed to the sliding motion. This equilibrium condition identifies the maximum static residual displacement

$$d_{\text{rm}} = \mu_d \frac{N}{K_p} = \mu_d R_{\text{eff}} \tag{2}$$

which represents the upper bound of the actual residual displacement d_{res} at the end of the motion, i.e., $-d_{\text{rm}} < d_{\text{res}} < d_{\text{rm}}$. From Eq. (2) it emerges that the maximum static residual displacement is proportional to the dynamic friction coefficient times the effective radius of curvature, and consequently, the re-centering capability of the CSS is not affected by the weight of the structure. An important parameter determining the re-centering capability of the isolation system has been

recognized to be the ratio $d_{\mathrm{cd}} / d_{\mathrm{rm}}$ [27], [28], with d_{cd} denoting the design seismic displacement. According to the Eurocode 8 (EC8) [37], [38] the isolation system has a satisfactory re-centering capability provided the following condition is satisfied

$$\frac{d_{\mathrm{cd}}}{d_{\mathrm{rm}}} \geq \delta \tag{3}$$

where δ is a numerical parameter whose recommended value is 0.5 [37]. In Eq. (3) the maximum residual displacement d_{rm} is an inherent property of the isolation system, while the design displacement d_{cd} depends also on the spectral characteristics of the seismic ground motion. As an example, ground motions with directivity effects (asymmetric accelerograms) like pulse-like excitations occurring in near-fault earthquakes may amplify the residual displacements due to an insufficient re-centering capability of the isolation system [39]. For CSSs the value $\delta = 0.5$ was demonstrated to be not sufficiently conservative [30], whereas values of $d_{\mathrm{cd}} / d_{\mathrm{rm}} > 2.5$ were found to produce negligible residual displacements ($d_{\mathrm{res}} < 0.1 d_{\mathrm{max}}$) [28], [31].

Assuming a cyclic motion of the CSS with symmetric amplitude d_{cd} (design displacement of the isolation system) and taking into account Eq. (2), the effective damping can be calculated in terms of the maximum residual displacement d_{rm} as follows

$$\xi_d = \frac{2}{\pi} \cdot \frac{\mu_d R_{\mathrm{eff}}}{\mu_d R_{\mathrm{eff}} + d_{\mathrm{cd}}} = \frac{2}{\pi} \cdot \frac{1}{1 + (d_{\mathrm{cd}} / d_{\mathrm{rm}})} \tag{4}$$

where the ratio $d_{\mathrm{cd}} / d_{\mathrm{rm}}$ indicates the re-centering capability of the CSS as per Eq. (3). Therefore, systems having high re-centering capability are associated with lower energy dissipation and hence larger displacements.

For the thermoplastic materials used for the sliding pad of CSSs, the dynamic friction coefficient varies with contact pressure, sliding velocity and temperature at the sliding interface [40]-[43]. In this study, for simplicity, the friction coefficient is assumed to be a function of the sliding velocity

only according to the well-established exponential law [44]

$$\mu_d = \mu_{HV} - (\mu_{HV} - \mu_{LV}) \cdot \exp(-\alpha \dot{d}) \tag{5}$$

where μ_{LV} and μ_{HV} are the friction coefficients at low and high velocities, respectively, and a (having unit of inverse of velocity) represents a rate parameter governing the transition from μ_{LV} to μ_{HV} [36]. As already noted in [30], while the parameter μ_{HV} is important during the strong motion phase of the earthquake for the determination of the maximum displacement $d_{\max}$ of the isolation system, during the coda stage the residual displacement is affected by the parameter μ_{LV} governing the low velocity motion of the CSS. Therefore, the value $\mu_d = \mu_{LV}$ can be assumed in the calculation of the maximum static residual displacement d_{rm} in Eq. (2) where the equilibrium of forces in the quasi-static condition is considered

$$d_{\mathrm{rm}} = \mu_{LV} \cdot R_{\mathrm{eff}} \tag{6}$$

Based on the previous Eq. (4), it emerges that energy dissipation and re-centering capability of CSS are two competing aspects. It seems, therefore, reasonable to introduce energy dissipation not throughout the range of displacement, but only beyond a certain displacement threshold in order to reduce the displacement demand while guaranteeing a high re-centering behavior. The introduction of a gap damper in combination with low-friction CSSs triggers such desired additional energy dissipation while not modifying the re-centering behavior underlying the low value of the friction coefficient.

3. HYSTERETIC GAP DAMPER

3.1. Conventional realization scheme

The working principle of a combined system comprising isolators and gap dampers is schematically shown in Figure 2. Whereas the CSSs are supposed to provide the classical functions

of the isolation system (i.e. support the gravity load of the superstructure, accommodate horizontal displacements with minimum resistance, provide a certain energy dissipation and the re-centering capability), the gap dampers introduce additional energy dissipation only when the displacement exceeds a given threshold or "initial gap" while not being engaged otherwise [32]-[34]. In real cases, isolation devices are subjected to the effect of three-dimensional acceleration time histories. Nevertheless, the validity of the proposed solution (CSS + gap damper) is not affected by the multi-directional nature of the earthquake ground motion. Considering this is a pilot study aimed at assessing the feasibility of the combined base-isolation system, the theoretical concepts and the numerical analyses reported in this paper will be limited to the simple case of unidirectional seismic excitation: the isolation system is subjected to a unidirectional motion and the gap dampers are placed along such direction of motion. For seismic applications involving cycling loading, two gap damper elements are installed. The gap dampers are connected to the isolation system through a rigid frame, represented by a square steel element surrounding the central isolation nub, according to a scheme previously proposed in [33], [34]. In particular, Figure 2 shows a stepwise analysis of the kinematics and the corresponding reaction force of the gap damper system. The isolation nub is initially centered with respect to the rigid frame, separated at either side by an initial gap d_{gap}, so that the isolation system is not affected by the presence of the gap dampers in the range of displacements $-d_{\text{gap}} < d < d_{\text{gap}}$. The gap dampers provide zero reaction force until a certain threshold displacement equal to d_{gap} is attained (step 1). From this displacement onwards, an elastic-perfectly plastic behavior is assumed (hysteretic gap damper). The ability of controlling the reaction force (and hence the engagement of a dissipation mechanism) in relationship to the amplitude of the displacement is termed "phased behavior" in previous papers [32]-[34]. In this regard, the nomenclature "gap damper" or "phased device" is often interchanged in the literature.

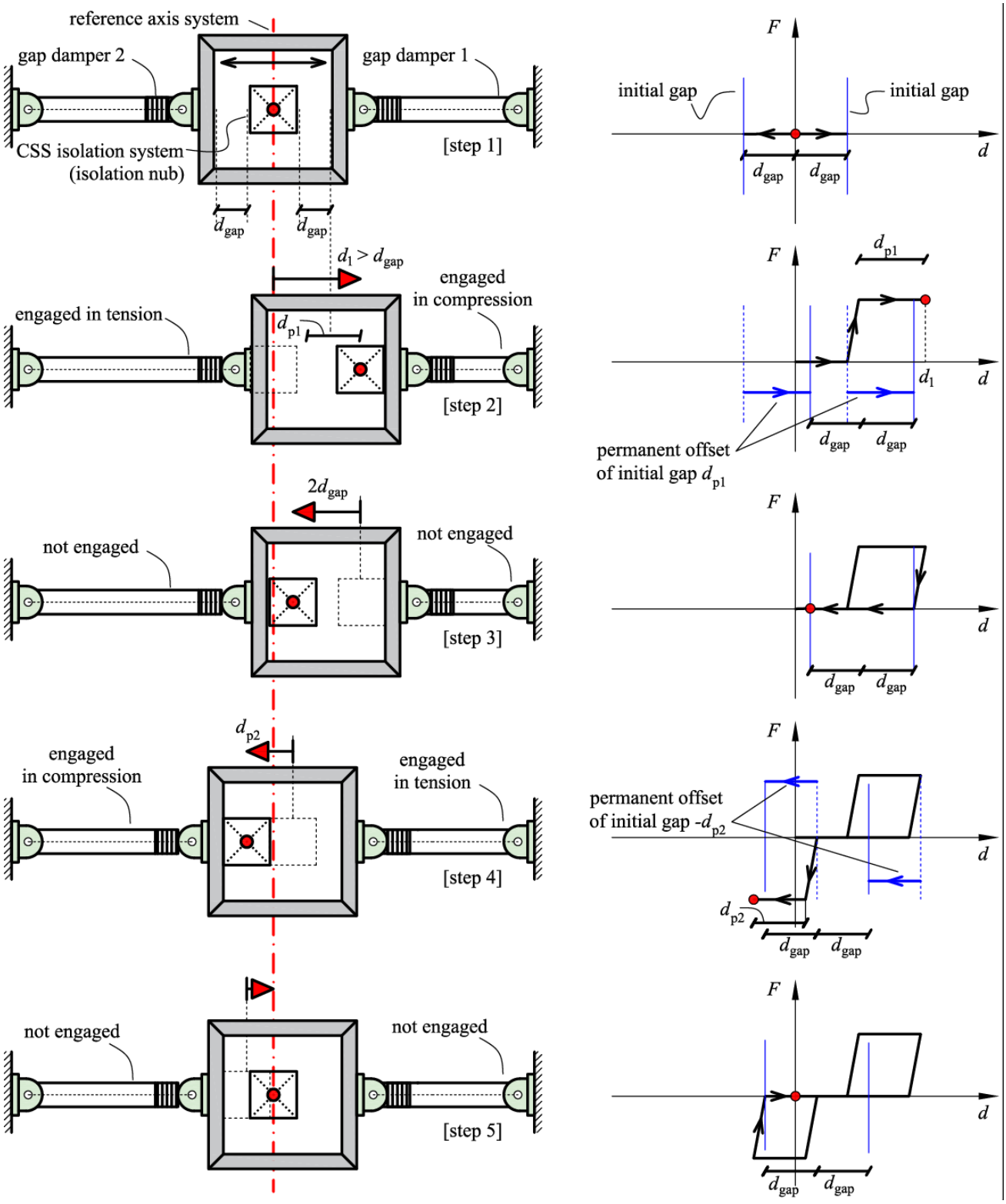

Figure 2 Conventional layout of isolation system combined with gap dampers (scheme proposed in [33], [34])

For a positive displacement $d_1 > d_{gap}$ gap damper 1 is engaged in compression while gap damper 2 is engaged in tension. When the motion reverts its direction, a portion of the total displacement d_1 is

recovered whereas a permanent deformation of the gap damper d_{p1} causes a shift of the initial gap towards the right (step 2). This means that gap dampers will be subsequently engaged at a displacement $d_{p1} - d_{gap}$. In the subsequent step 3, at a displacement $-2\,d_{gap}$ from the maximum position on the right side, the isolation nub comes into contact with the rigid frame and engages the gap dampers anew. It must be noted that that when the isolation system moves to the left the gap dampers will be engaged for a positive displacement (in the reference axis system). This occurs because the permanent offset of the initial gap during step 2 is assumed to be $d_{p1} > d_{gap}$. The effects of the residual displacement on the overall system performance were studied by Zargar et al. [34]. A subsequent displacement to the left (step 4) entails the engagement of the gap dampers and the accumulation of a permanent deformation in this direction, equal to d_{p2}. Therefore, at the next motion reversal the initial gap is shifted by a quantity $d_{p1} - d_{p2}$, which implies that the triggering of the gap damper system is affected by the permanent deformations accrued during the response history. Moreover, the shift of the initial gap may introduce a force that opposes to the re-centering of the CSS isolation system. In particular, for ground motions with high directivity effects (i.e. asymmetric accelerograms), the permanent deformation may be large. At the end of the ground motion the rigid frame is shifted in one direction (for instance, to the right side), and the re-centering action of the CSS during the coda stage is opposed by a non-zero damping force produced by the gap dampers in the neighborhood of the origin of the reference system. Consequently, the shift of the initial gap may negatively affect the re-centering capability of the isolation system for asymmetrical accelerograms.

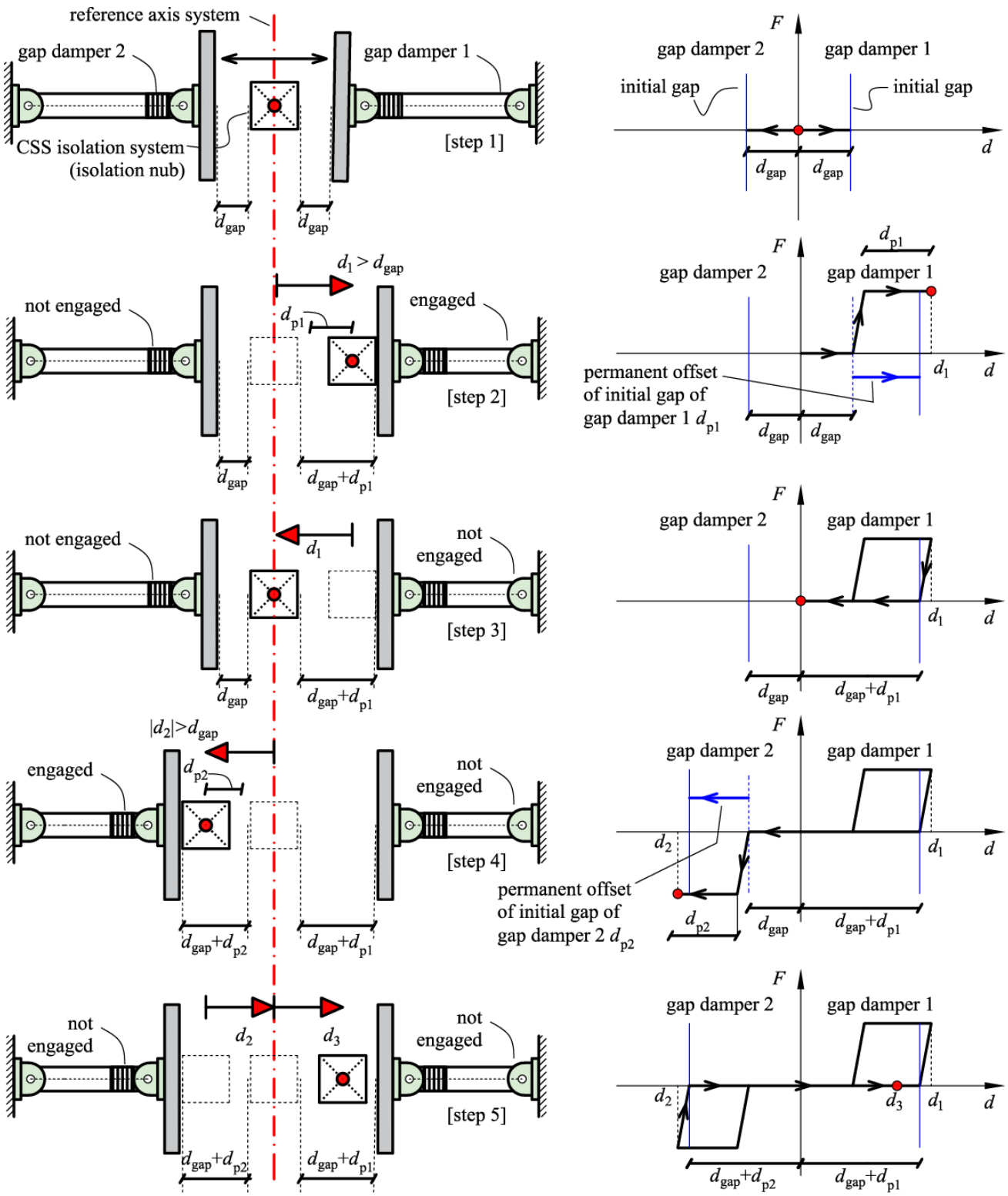

Figure 3 Alternative layout of isolation system combined with gap dampers (scheme proposed in this study)

3.2. Proposed realization scheme

An alternative layout for the use of gap dampers is proposed in this paper and sketched in Figure

3. Two gap dampers are located at an initial distance d_{gap} on either side of the isolation system, but, unlike in the previous layout, the rigid frame surrounding the isolation nub is replaced by two independent steel walls which permit to separately engage either gap damper depending on whether the isolation system moves to the left or to the right. Therefore, gap dampers 1 and 2 are not engaged simultaneously, but are triggered one at a time as "compression-only" element when the isolation nub is in contact with either steel wall. A stepwise representation of the operation of the gap damper system is schematically shown in Figure 3. In the range of displacements $-d_{\text{gap}} < d < d_{\text{gap}}$ no gap damper is engaged and the reaction force is zero (step 1). Owing to a displacement of the isolation system of $d_1 > d_{\text{gap}}$ to the right, gap damper 1 is engaged (in compression) while gap damper 2 is not engaged (step 2). The permanent component d_{p1} of the total displacement d_1 produces a shift of the initial gap of gap damper 1 (which changes from d_{gap} to $d_{\text{gap}} + d_{\text{p1}}$), while the initial gap of gap damper 2 is not changed. After motion reversal, for $0 \le d \le d_{\text{gap}} + d_{\text{p1}}$ (where $d = 0$ is the origin of the reference axis system), gap damper 1 is no longer engaged (step 3). Moving now from the origin to the left side of a quantity $|d_2| > d_{\text{gap}}$ (step 4), gap damper 2 is activated, while gap damper 1 is not. The permanent component d_{p2} of the total displacement d_2 produces now a shift towards left of the initial gap of gap damper 2. The effect of the shifts of the initial gap occurred in steps 1-4 has increased the range of "no-engagement" displacement from $[-d_{\text{gap}}, d_{\text{gap}}]$ to $[-d_{\text{gap}} + d_{\text{p2}}, d_{\text{gap}} + d_{\text{p1}}]$, and hence, when the isolation system moves towards right of a quantity $d_2 + d_3$ with $d_{\text{gap}} < d_3 < d_{\text{p1}}$, gap damper 1 is not engaged. The proposed gap damper layout does not impair the re-centering capability of the isolation system, even for asymmetrical accelerograms with pronounced directivity effects, because no reaction force is produced by the gap damper during free vibration of the CSS in the neighborhood of the origin of the reference system. However, the shift of the initial gap may be detrimental in case of aftershocks, because the engagement of the gap damper is delayed. In the

sequel of the paper, we will refer to this phenomenon as “cumulative damage” of the gap damper system. In the following subsection, a procedure for the design of the hysteretic gap damper for the proposed combined base-isolation layout is presented.

3.3. Energy-based design of the hysteretic gap damper

An elastic-perfectly plastic behavior of the hysteretic gap damper is assumed, with initial stiffness K_i and yield force F_y. In this study, the initial stiffness of the gap damper is not an explicit design variable since the yield displacement is set to $d_y = 1\,\text{mm}$, which is an average reasonable value among those measured on a wide variety of steel hysteretic dampers [45]. Therefore, the design of the gap damper consists in selecting the yield force F_y and the gap displacement d_{gap}. With the aid of Figure 4, a performance-oriented energy-based design procedure is developed [46]. In particular, the top of Figure 4 shows a typical force-displacement loop of a low-friction CSS with design displacement d_{cd}. The aim of the gap damper is to provide supplemental energy dissipation such that the displacement demand of the CSS is reduced from d_{cd} to a target displacement d_{red}. Without loss of generality, the reduced displacement d_{red} can be expressed through a reduction factor RF multiplying the displacement demand of the CSS alone, i.e.

$$d_{red} = RF \cdot d_{cd} \tag{7}$$

where $0 < RF < 1$. As an example, the reduction factor RF can be assumed equal to the ratio between the displacement demand of a high-friction CSS and the displacement demand of the actual low-friction CSS, being the radius of curvature the same

$$RF = \frac{d_{cd}^{\text{high-friction}}}{d_{cd}^{\text{low-friction}}} \tag{8}$$

In this way, the gap damper would ideally keep the displacement demand of the low-friction CSS to the same level as that of high-friction CSS.

According to the proposed design procedure, the supplemental energy dissipation provided by the gap damper (E_{damper} in Figure 4) is set equal to the energy E_{red} that would be dissipated by the CSS in one cycle while moving from d_{red} to d_{cd} (dashed area shown in the top part of Figure 4).

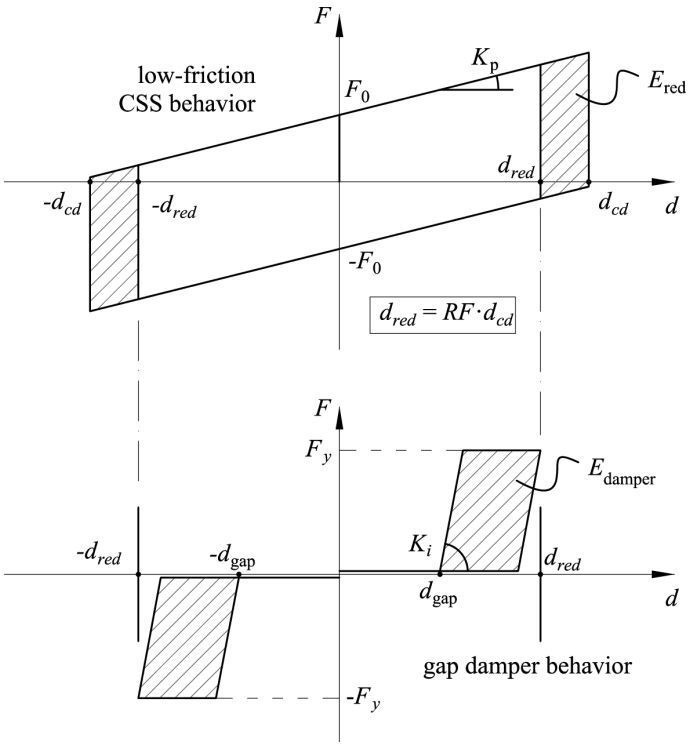

Figure 4 Force-displacement curve of low-friction CSS (top) and gap damper (bottom)

This term is easily calculated as follows

$$E_{\text{red}} = 4F_0(1 - RF)d_{cd} \tag{9}$$

On the other hand, by assuming an elastic-perfectly plastic behavior, the energy dissipated by the gap damper with initial gap $d_{\text{gap}} < d_{red}$ during a complete cycle of amplitude d_{red} is given by

$$E_{\text{damper}} = 2F_y(RF \cdot d_{cd} - d_{\text{gap}} - d_y) \tag{10}$$

Equating the energy terms in Eqs. (9) and (10) gives a closed-form expression of the yield force of the gap damper F_y according to the proposed energy-based design procedure

$$F_y = \frac{2F_0\left(1-RF\right)d_{cd}}{RF\cdot d_{cd} - d_{\text{gap}} - d_y} = 2\mu_{HV}N\frac{\left(1-RF\right)}{RF-\left(\frac{d_{\text{gap}}}{d_{cd}}\right)-\left(\frac{d_y}{d_{cd}}\right)} \tag{11}$$

where it has been assumed $F_0 = \mu_{HV}N$. It must be noted that the yield displacement of the gap damper d_y affects the design of the gap damper only for very low values of d_{cd}, whereas in typical conditions the ratio $d_y / d_{cd} \ll 1$ so that the influence of d_y in the calculation of F_y becomes negligible.

Beside the yield force F_y, another fundamental parameter for the design of the gap damper is the displacement threshold d_{gap} that triggers the activation of the device. In previous implementations [32]-[34] the initial gap was assigned so that the supplemental damping was provided only in extreme earthquakes In the present work, different options of the initial gap are explored within a parametric study, and the influence of d_{gap} on the displacement demand and re-centering capability of the combined isolation layout is investigated.

4. NUMERICAL ANALYSES

The seismic performance of the proposed base-isolation system is assessed through nonlinear response history analyses (NRHAs) performed on a single degree of freedom (SDOF) system, postulating a rigid-body behavior for the superstructure. The earthquake excitation consists of a suite of historically recorded acceleration time histories. The NRHAs were carried out with the structural analysis program OpenSees v. 2.5.4 [47], using the "Single Friction Pendulum Bearing Element" [48] to describe the hysteretic behavior of the CSS, with a velocity-dependent friction model as reported in Eq. (5), and the "elastic-perfectly plastic gap material" (compression only) to describe the hysteretic behavior of the gap damper [48]. Only one horizontal component of the earthquake excitation was applied to the SDOF, whereas the vertical component of the seismic input was not included in this study. Therefore, the influence of the normal force on the friction coefficient was

disregarded. Also, the influence of the heating phenomena on the degradation of the friction coefficient was neglected. A constant vertical load equal to $N = 1000\,\text{kN}$ was considered in the NHRAs for computing the corresponding mass of the isolation system, as well as the restoring stiffness of the CSS and the yield force of the gap damper according to Eq. (11). An elastic-plastic bilinear model for the CSS is assumed, with initial stiffness assumed equal to $K_i = 100K_p$ in order to minimize the elastic deformation of the bearing [31].

4.1. CSS parameters and selection of ground motion records

Based on the energy-based design procedure illustrated in Section 3.3, the goal is to compare the response of the conventional isolation system with CSS alone against the response of the base-isolation system with CSS combined with gap dampers. In the parametric study, different radii of curvature and different friction coefficients of the CSS were analyzed in order to cover a typical range of devices available on the market. In particular, three values of the radius of curvature (R_1, R_2, R_3), corresponding to CSS un-damped fundamental periods of 2.98, 3.75, 4.49 s, and three friction classes (f_1, f_2, f_3), representative of low friction (LF), medium friction (MF), and high-friction (HF) sliding materials were considered (Table 1). A ratio of the high-velocity to low-velocity friction coefficient $\mu_{HV} / \mu_{LV} = 2.5$ was assumed for the three friction classes, and the rate parameter α governing the transition between the two friction values was set to $\alpha = 0.0055\,s/\text{mm}$, according to the literature [28].

Table 1 CSS and gap damper mechanical properties examined in the parametric study

Effective radius of curvature R_{eff}			Friction coefficient $\begin{pmatrix}\mu_{LV}\\ \mu_{HV}\end{pmatrix}$			Initial gap ratio $d_{\text{gap}} / d_{\text{red}}$		
R_1 [mm]	R_2 [mm]	R_3 [mm]	f_1	f_2	f_3	GF_1	GF_2	GF_3
2200	3500	5000	$\begin{pmatrix}0.02\\ 0.05\end{pmatrix}$	$\begin{pmatrix}0.035\\ 0.0875\end{pmatrix}$	$\begin{pmatrix}0.05\\ 0.125\end{pmatrix}$	25%	50%	75%

In the proposed design procedure of the hysteretic gap damper, the displacement demand of the

isolation system with CSS alone is assumed to be known from iterative spectral analyses or nonlinear dynamic analyses. In particular, it is assumed that the proposed isolation system is installed in Lamezia Terme, Italy (latitude 38.57°, longitude 16.18°), where the seismic hazard map is provided by the Italian building code NTC2018 [49]. A strategic structure is considered with nominal life of $V_N = 100\,\text{years}$ and functional class IV corresponding to an amplification factor $C_U = 2.0$. The resulting reference life of the structure is $V_R = V_N \cdot C_U = 200\,\text{years}$. According to the performance-based design, two distinct performance requirements corresponding to two distinct limit states are considered depending on the intensity level of the seismic excitation. The acronyms of these two limit states in the Italian building code [49] are "SLD" and "SLC", the former denoting a serviceability limit state with damage-limitation requirement and a 63% probability of exceedance during the reference life of the structure (return period of 201 years), and the latter corresponding to the maximum considered earthquake with no-collapse requirement and a 5% probability of exceedance during V_R (return period of 2475 years). A topography condition T_1 and a soil type A were assumed. These assumptions led to a peak ground acceleration (PGA) equal to 0.498 g and to 0.181g for SLC and SLD, respectively. For each limit state, a suite of seven independent spectrum-compatible natural records was selected by means of the software REXEL v. 3.5 [50] from the European strong-motion database [51] among events having magnitude $6 \le M_w \le 7$ for SLC, and $5.5 \le M_w \le 6$ for SLD, while the epicentral distance was set to $R_{ep} \le 30\,\text{km}$ for both limit states. The spectrum-matching criterion was enforced in the range [0.15-4] s, with lower and upper tolerance equal to 10%. A scale factor (SF) was applied to each acceleration time history in order to match the target acceleration response spectrum at 5% damping. Details of seven records selected, along with the corresponding original PGA, SF and scaled PGA, are listed in Table 2 and Table 3 for the SLD and SLC, respectively.

Table 2 Ground motion records selected for seismic analyses at SLD

Waveform ID (component)	Earthquake	Station ID	Date	M_w	R_{ep} [km]	PGA [g]	SF	scaled PGA [g]
5272 (x)	Mt. Vatnafjoll	ST2487	25/05/1987	6.0	24	0.033	5.51	0.181
368 (x)	Lazio Abruzzo	ST143	07/05/1984	5.9	22	0.064	2.82	0.181
1891 (y)	Kranidia	ST1320	25/10/1984	5.5	23	0.026	6.95	0.181
5270 (x)	Mt. Vatnafjoll	ST2486	25/05/1987	6.0	25	0.031	5.87	0.181
646 (y)	Umbria Marche	ST234	14/10/1997	5.6	17	0.029	6.35	0.181
642 (x)	Umbria Marche	ST225	14/10/1997	5.6	23	0.053	3.39	0.181
410 (y)	Golbasi	ST161	05/05/1986	6.0	29	0.055	3.30	0.181
			mean	**5.8**	**23.3**	**0.0415**	**4.88**	**0.181**

Table 3 Ground motion records selected for seismic analyses at SLC

Waveform ID (component)	Earthquake	Station ID	Date	M_w	R_{ep} [km]	PGA [g]	SF	scaled PGA [g]
198 (x)	Montenegro	ST64	15/04/1979	6.9	21	0.181	2.75	0.498
6335 (x)	South Iceland	ST2557	21/06/2000	6.4	15	0.127	3.92	0.498
4674 (x)	South Iceland	ST2486	17/06/2000	6.5	5	0.318	1.57	0.498
4675 (y)	South Iceland	ST2487	17/06/2000	6.5	13	0.156	3.19	0.498
55 (y)	Friuli	ST20	06/05/1976	6.5	23	0.316	1.58	0.498
128 (y)	Friuli	ST36	15/09/1976	6.0	28	0.070	7.13	0.498
6341 (x)	South Iceland	ST2497	21/06/2000	6.4	20	0.051	9.69	0.498
			mean	**6.5**	**17.9**	**0.174**	**4.26**	**0.498**

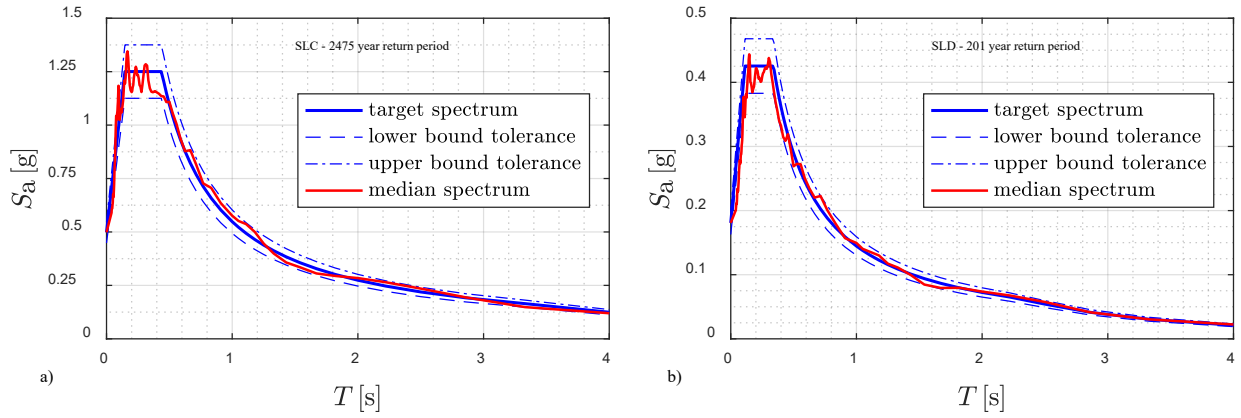

Figure 5 Comparison between the target response spectrum for the installation site and the median response spectrum of the seven selected independent records for the two limit states: a) SLC; b) SLD

The target response spectrum, and the median response spectrum of the suite of records are compared to one another in Figure 5.

The influence of d_{gap} on the seismic performance of the combined base isolation system is

investigated by considering different ratios in proportion to the reduced displacement demand d_{red}. Namely, three gap factor ratios d_{gap}/d_{red} (GF_1, GF_2, GF_3) equal to 25%, 50% and 75% are chosen, as listed in Table 1, which assume the engagement of the gap damper at one quarter, one half and three fourth of the target reduced displacement demand. The nomenclature adopted to identify the base-isolation system is $R_i f_j$ (with i=1,2,3; j=1,2,3) for the conventional isolation system with CSS alone, and $R_i f_j GF_k$ (with i=1,2,3; j=1,2; k=1,2,3) for the CSS + gap damper combined isolation layout. Therefore, 9 different combinations of CSS properties and 18 different combinations of CSS + gap damper properties are studied.

4.2. Time history response of CSS isolation system combined with gap damper

In this subsection, the response of the combined CSS + gap damper isolation layout is illustrated and compared to the response of the conventional CSS isolation system. Reference is made to the CSS having radius of curvature $R_2 = 3500\,\text{mm}$. Two ground motion records are considered, one for the SLC and one for the SLD, in order to assess the performance for either high-intensity or low-intensity ground motions. In particular, the South Iceland earthquake (ID 6341, station ST2497) and the Golbasi earthquake (ID 410, station ST161) are considered as representative records for the SLC and SLD, respectively.

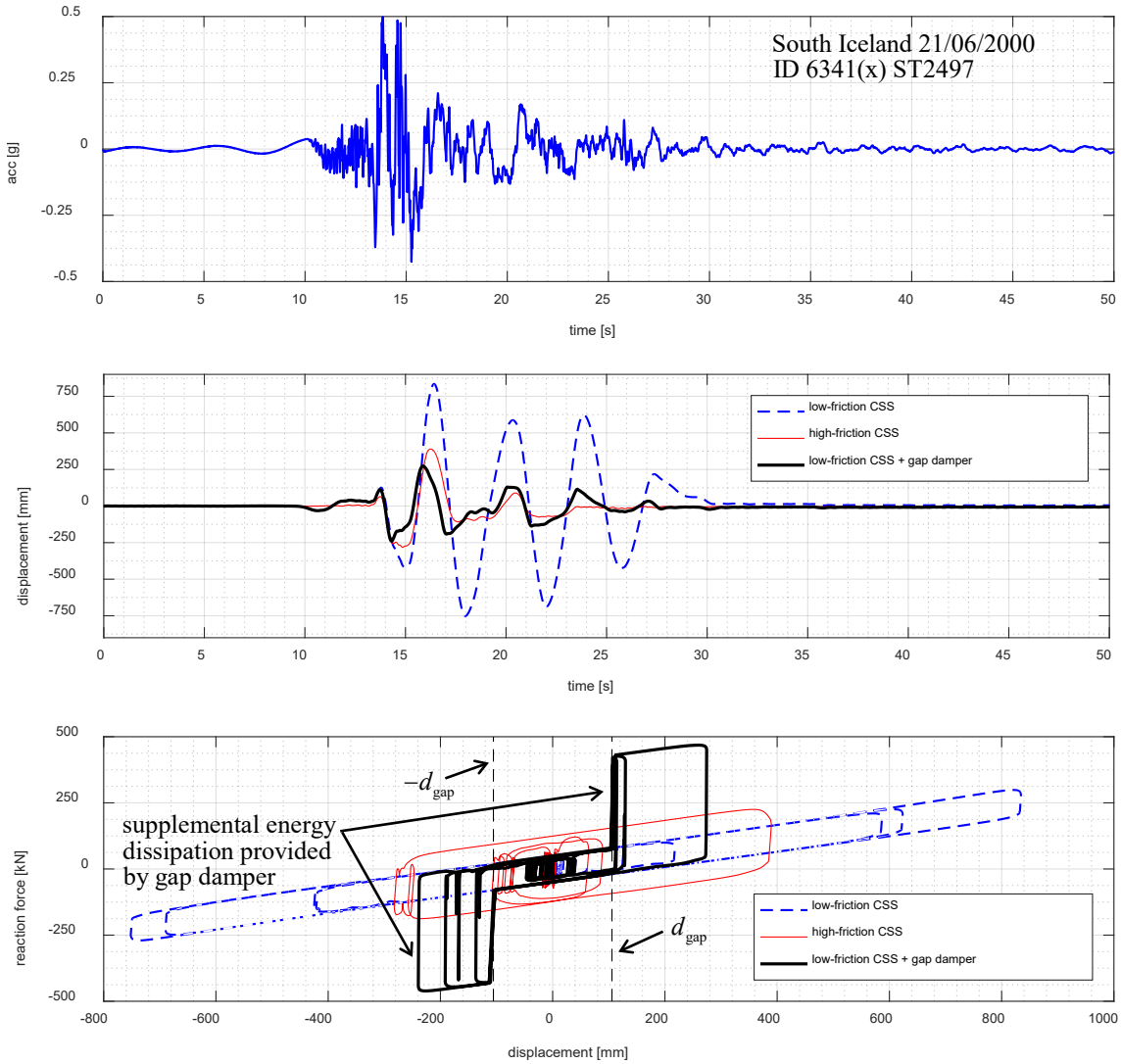

Figure 6 Response to high-intensity ground motions: acceleration time history of the South Iceland earthquake (top), displacement response of different isolation systems (middle) and corresponding force-displacement loops (bottom)

In Figure 6 the acceleration history of the South Iceland earthquake is depicted, along with the response in terms of displacement history and force-displacement loops. Three different isolation systems are compared, namely the low-friction CSS system (f_1), the high-friction CSS system (f_3) and the novel system combining low-friction CSS (f_1) with gap dampers. The parameters of the gap damper were selected according to the energy-based procedure described in subsection 3.3, assuming the displacement demand of the high-friction CSS (defined as the mean response for the 7 records at SLC) as the target displacement demand. From Figure 6, it is evident that the combined isolation system with gap dampers is able to substantially reduce the displacement demand in comparison with

the low-friction CSS. The resulting displacement is comparable to the displacement of the high-friction CSS (the discrepancy between the two values of displacement are due to the fact that the design procedure is applied considering the average displacement demand for the suite of 7 records, not the single record). The force-displacement loops calculated for the combined isolation system confirms that the gap damper is able to provide a supplemental energy dissipation when the displacement exceeds the initial gap d_{gap} in either direction (phased behavior).

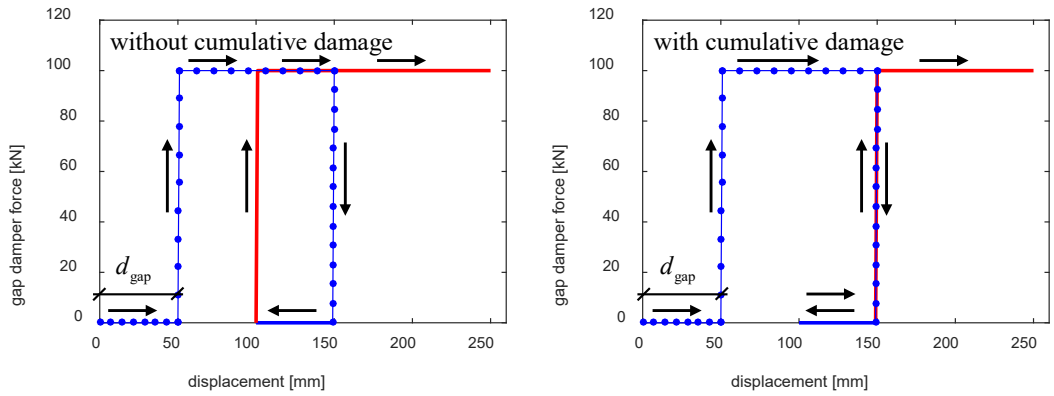

Figure 7 Force-displacement relationship of the elastic-perfectly plastic gap material implemented in OpenSees without and with cumulative damage (adapted from OpenSeesWiki [48])

The diagrams shown in Figure 6 refer to a gap damper without cumulative damage. This assumption implies that the performance of the gap damper at the first and at the subsequent engagements is the same because the initial gap is not affected by accrual of plastic deformation in previous cycles. The effect of the cumulative damage on the seismic performance of the gap damper can be simulated in the numerical analyses by switching on and off the "damage" string in the elastic-perfectly plastic gap material in OpenSees [47]. The corresponding force-displacement relationships for the gap damper without and with cumulative damage are represented in Figure 7.

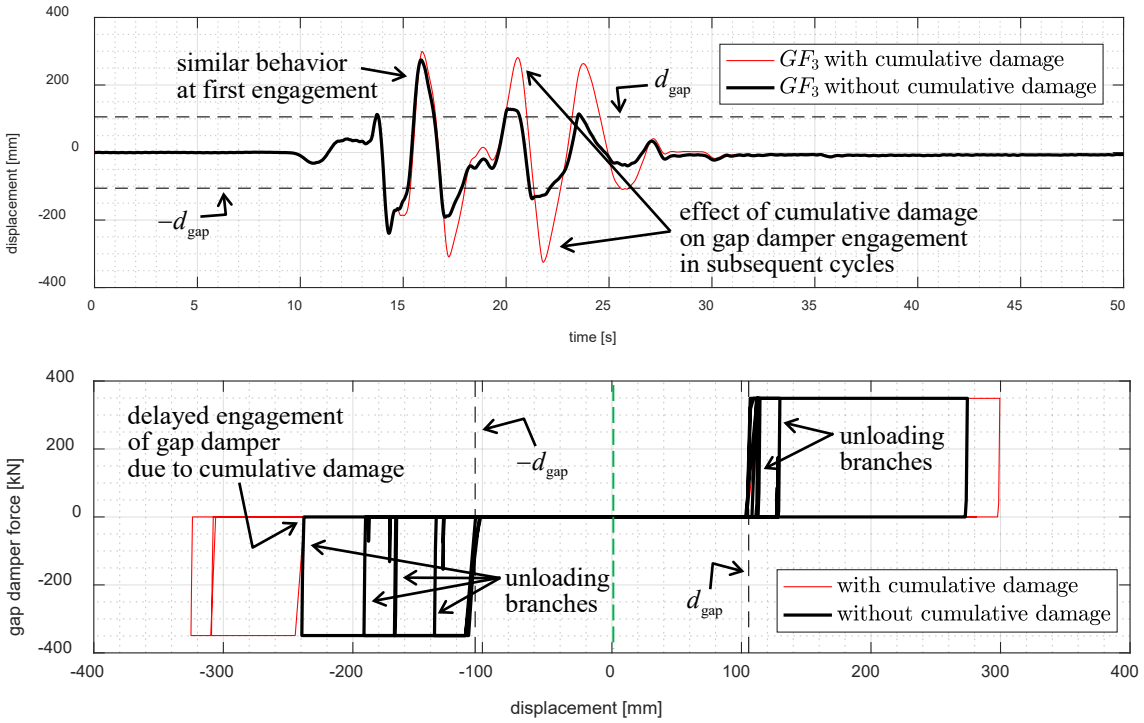

Figure 8 Response to high-intensity ground motions: effect of cumulative damage on the displacement mitigation effect of gap dampers (top) and corresponding force-displacement loops of gap dampers (bottom)

In order to demonstrate the influence of the cumulative damage on the performance of the gap damper, in Figure 8 the responses of the combined isolation system either with or without cumulative damage of the gap damper are compared to each other in terms of displacement history and hysteretic loops. It is shown that the cumulative damage may negatively affect the performance of the gap damper in terms of displacement mitigation, because of the engagement at larger displacements in subsequent cycles. Nevertheless, in the reported example, even in presence of cumulative damage of the gap damper the displacement demand of the isolation system combined with gap dampers is significantly smaller than the demand of the system with low-friction CSS alone.

Another important parameter in the design of the gap damper system is the gap factor GF, which is related to the threshold displacement for engagement. The displacement responses corresponding to the three gap factors GF_1, GF_2, GF_3 (Table 1) are shown in Figure 9: the most effective choice corresponds to gap factor GF_3, which indicates an initial gap equal to 75% of the reduced

displacement demand. This is reasonable for the system with cumulative damage, where the permanent deformation accumulated during the seismic movement decreases with increasing of the threshold displacement. Therefore, a large gap factor implies that the gap damper is engaged only during the strong motion phase of the accelerogram, where the extreme displacement is attained, whereas for smaller displacements the gap damper is not activated. On the contrary, a small gap factor would entail multiple engagements of the gap damper, even during small movements, and a consequent accrual of plastic deformations. According to the energy-based design procedure, the same amount of supplemental energy dissipation is assumed for the three gap factors, therefore systems having a lower gap factor have necessarily a lower value of yield force and higher displacements. An increase of the gap factor consequent to cumulative damage implies that larger displacements should be accommodated to dissipate the same amount of energy, as can be seen in the force-displacement loops shown in Figure 9.

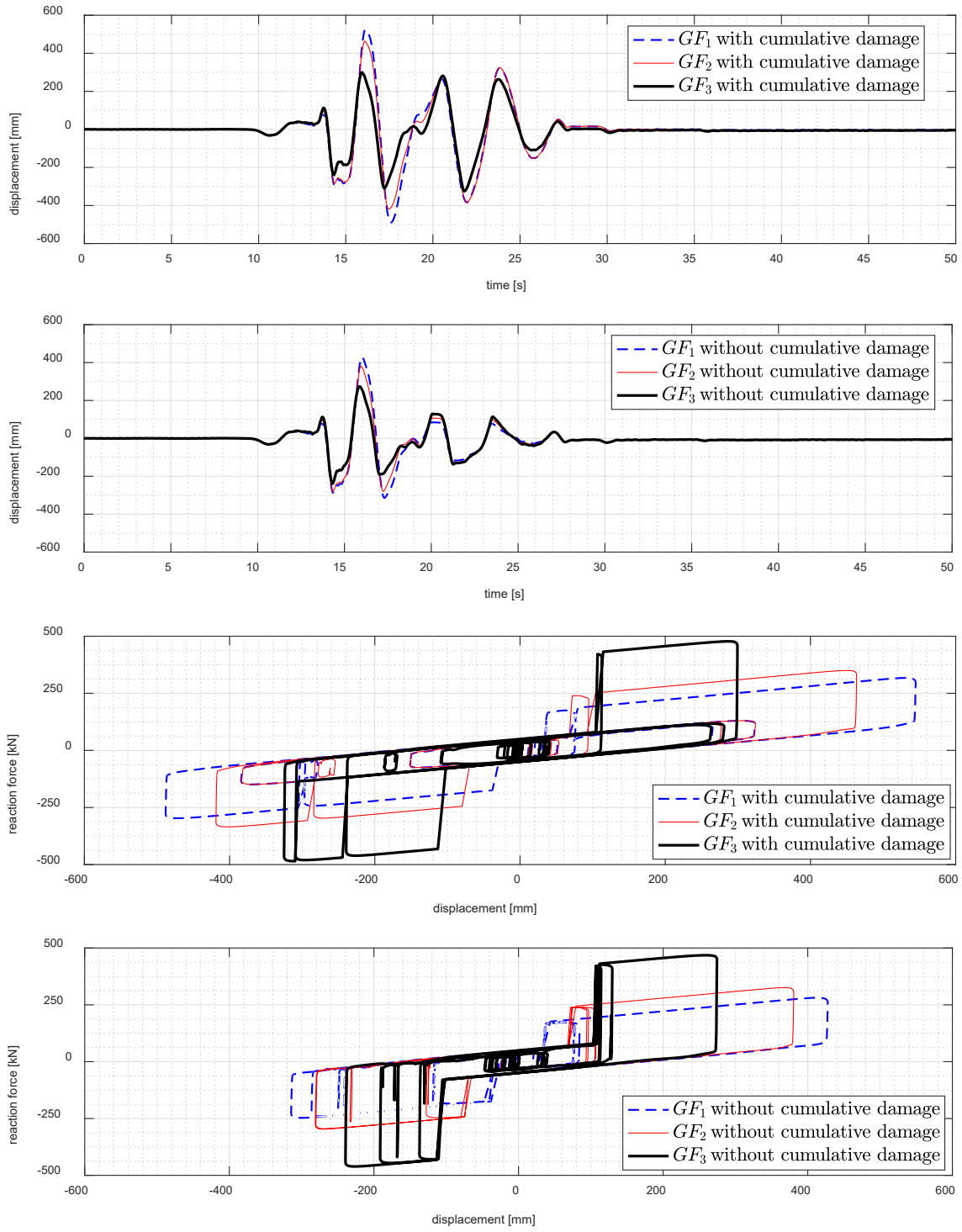

Figure 9 Response to high-intensity ground motions: effect of gap damper factor on displacement mitigation effect of gap damper with and without cumulative damage (top), and corresponding force-displacement loops of combined isolation system with and without cumulative damage (bottom)

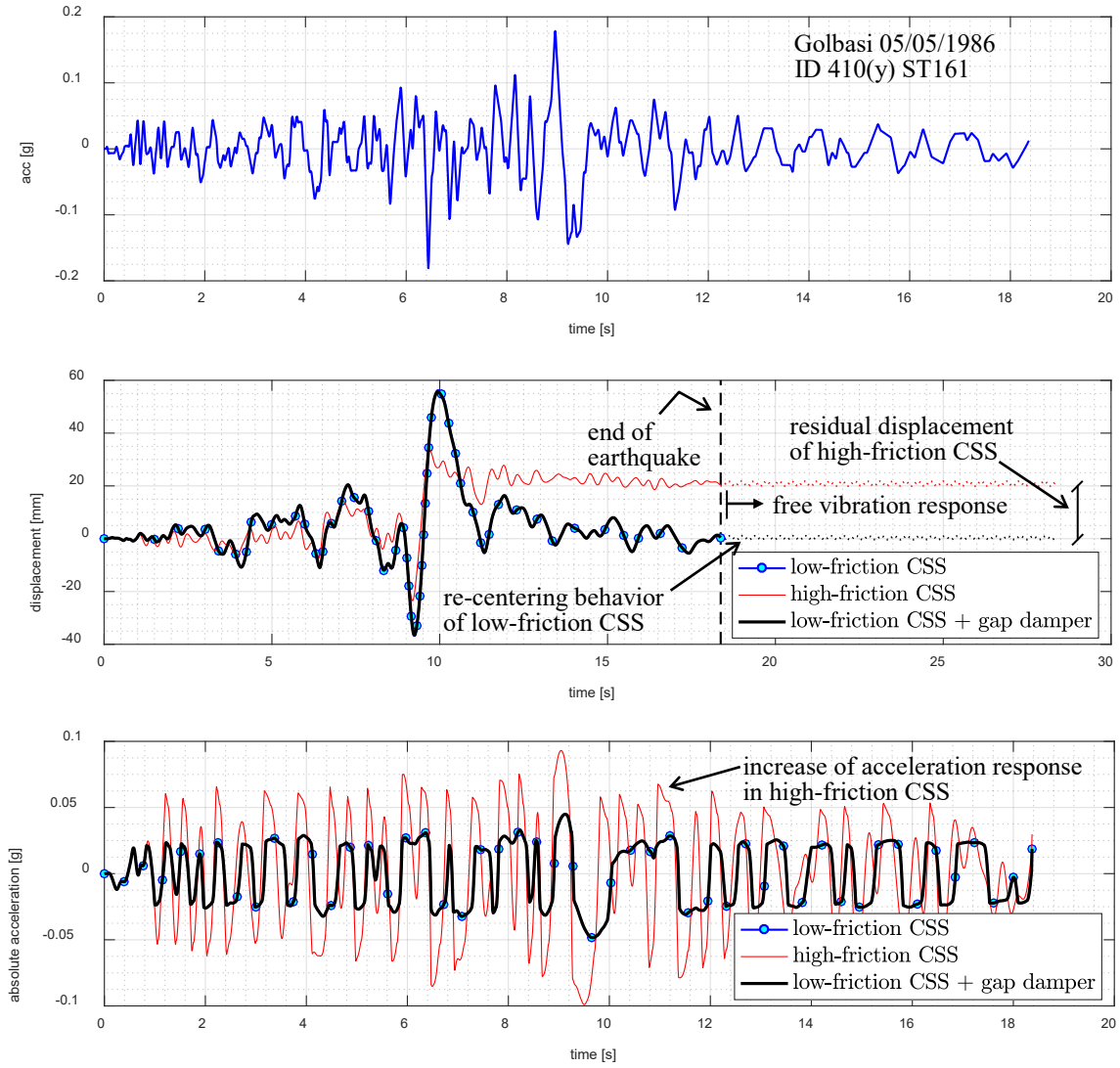

Figure 10 Response to lower-intensity ground motions: acceleration time history of the Golbasi earthquake (top), displacement response (middle) and absolute acceleration response (bottom) of different isolation systems

With regard to low-intensity ground motions, the acceleration history of the Golbasi earthquake is shown in Figure 10, along with the displacement and absolute acceleration responses for the three examined isolation systems. The displacement history is purposely reported over a longer time than the duration of the ground motion acceleration history, in order to assess the free vibration response and the corresponding residual displacement at the end of the earthquake event. It is noted that the residual displacement caused by low-intensity ground motions may be an issue for structures equipped with high-friction isolation systems. In the example, the residual displacement of the high-friction CSS is about 21 mm, which is more than 60% of the peak seismic displacement (32 mm). On

the other hand, the isolation system combined with gap dampers benefits from the good re-centering capability typical of low-friction CSS, which, as expected, has not been unpaired by the gap dampers according to the proposed realization scheme (Figure 3). Similar considerations can be made concerning the absolute acceleration response, as the peak accelerations for both the low-friction CSS and the combined system with gap damper is about one half of the value observed for the high-friction CSS.

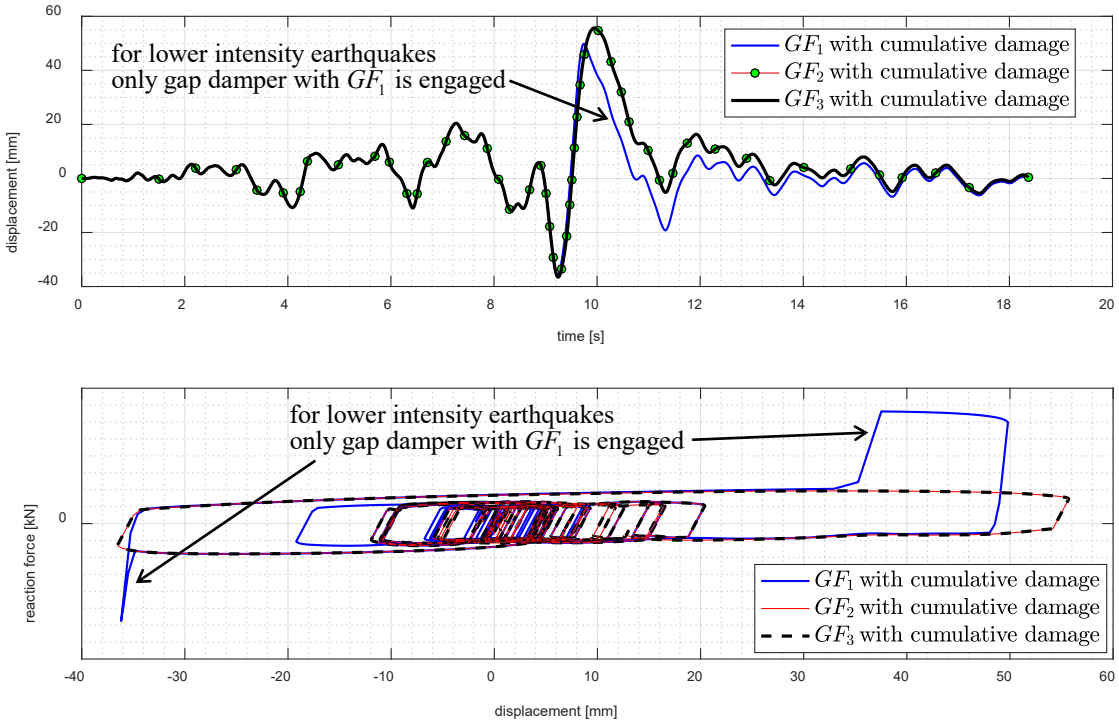

Figure 11 Response to lower-intensity ground motions: effect of gap damper factor on displacement mitigation effect of gap damper with cumulative damage (top) and corresponding force-displacement loops of combined isolation system (bottom)

These results highlight the beneficial effects of the phased behavior of the gap damper in eliminating undesirable effects associated with large amounts of damping provided by a high friction coefficient at low-intensity ground motions. In particular, the engagement of the gap dampers can be totally avoided during low-intensity ground motions by properly setting the gap factor. In Figure 11, it can be seen that the gap dampers are not engaged at all when either gap factor GF_2 or GF_3 are assumed, whereas it is partly engaged for gap factor GF_1. Although limited to the analysis of two earthquake records, these results suggest that GF_3 could be an appropriate gap factor to meet performance

requirements simultaneously for both high-intensity ground motions and low-intensity ground motions. More detailed considerations will be made in the next subsection by analyzing other CSS parameters and the entire suite of ground motion records.

4.3. Results of the parametric study

As already anticipated, different performance requirements are associated to the two limit states considered in this study: at SLC the goal is to achieve the collapse prevention (CP) performance level, while extensive damage and plasticization of structural and non-structural elements are allowed to occur; at SLD the goal is to achieve an immediate occupancy (IO) performance level for structural elements, with low-to-moderate damage of the non-structural elements. The two performance requirements are therefore checked for the base-isolation system accordingly. For the maximum considered earthquake at SLC, the isolators must be able to accommodate the displacement demand, which is the primary design parameter for the isolation system. For frequent earthquakes corresponding to SLD level, the acceleration induced in the isolated structure must be sufficiently low to prevent damage to non-structural elements [52], [53]. At either limit state, the re-centering capability is an important function of the isolation system, and the residual displacement must be checked in view of serviceability requirements and possible accrual of displacements in case of aftershocks or future events.

The results in terms of average maximum displacement ($d_{\max}$), average residual displacement normalized by $d_{\max}$ ($d_{\text{res}}/d_{\max}$), and average maximum absolute acceleration ($\text{acc}_{\max}$) over the seven earthquake records for both SLC and SLD are calculated for the isolation system with CSS only and for the proposed base-isolation layout combining CSS with gap dampers. The results for the conventional CSS isolation system without gap dampers are summarized in Figure 12.

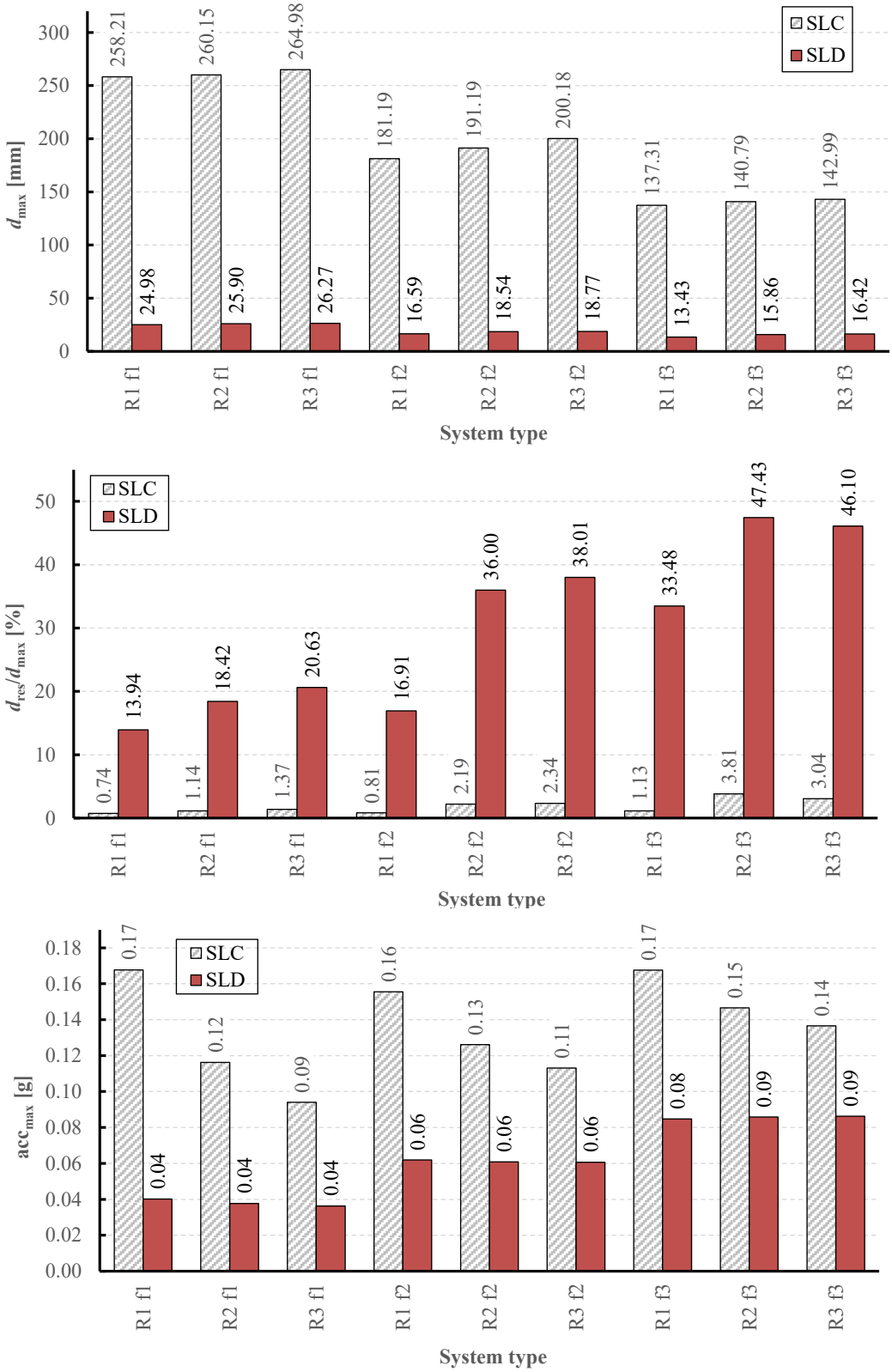

Figure 12 Seismic performance in terms of maximum displacement (top), residual displacement ratio (center) and maximum absolute acceleration (bottom) of the CSS isolation system with different values of radius of curvature and friction coefficient

As expected, the displacement demand is highly dependent on the friction coefficient, as the

maximum displacement decreases by about 40-45% when passing from f_1 to f_3. On the contrary, the radius of curvature has little influence, as $d_{\max}$ increases by less than 10% when passing from R_1 to R_3. The re-centering capability is affected by both the radius of curvature and the friction coefficient, as it depends on the parameter $d_{\mathrm{rm}} = \mu_d R_{eff}$. The poorest re-centering behavior is provided by systems having the largest radius of curvature in combination with the highest friction coefficient. This is more evident at SLD when the maximum displacement is small. As an example, at SLD the CSS isolation system $R_3 f_3$ has a residual displacement corresponding to $d_{\mathrm{res}} / d_{\max} = 46.1\%$, which means that the residual displacement is about 50% of the peak seismic displacement.

In order to highlight the advantages of the base-isolation layout made of CSS combined with gap dampers against the conventional CSS isolation system, the results are shown in a normalized format. For the displacement demand, the ratio $d_{\max} / d_{\max}^{\mathrm{HF}}$ is calculated, with $d_{\max}^{\mathrm{HF}}$ denoting the average displacement demand of the high-friction CSS (f_3 friction class). The average residual displacements are plotted in terms of the ratio $d_{\mathrm{res}} / d_{\mathrm{res}}^{\mathrm{LF}}$, with $d_{\mathrm{res}}^{\mathrm{LF}}$ denoting the average residual displacement achieved by the low-friction CSS (f_1 friction class), which provides the best re-centering capability. For the average maximum absolute acceleration, the ratio $\mathrm{acc}_{\max} / \mathrm{acc}_{\max}^{\mathrm{HF}}$ is calculated for both SLC and SLF, with $\mathrm{acc}_{\max}^{\mathrm{HF}}$ denoting the average maximum absolute acceleration of the high-friction CSS (f_3 friction class). Finally, the ratio $\mathrm{acc}_{\max} / \mathrm{acc}_{\max}^{\mathrm{LF}}$, with $\mathrm{acc}_{\max}^{\mathrm{LF}}$ denoting the average maximum absolute acceleration of the low-friction CSS, is also computed at SLD for additional considerations in terms of serviceability requirements for low intensity ground motions.

The results are shown in Figure 13, Figure 14, and Figure 15 for each of the 18 combinations of design parameters, including the three radii of curvature (R_1, R_2, R_3), the two friction coefficients (f_1, f_2) and the three gap displacements or engagement thresholds of the gap damper

(GF_1, GF_2, GF_3). Moreover, the influence of the cumulative damage of the gap dampers is assessed by reporting separate results corresponding to the configuration either with or without cumulative damage. By examining the results shown in the figures the following conclusions can be drawn:

1) The proposed isolation layout combining low-friction CSSs with gap dampers outperforms the conventional CSS isolation system for both the SLD and the SLC performance requirements. In particular, the proposed system is characterized by a reduced displacement demand at SLC, comparable to the demand provided by high-friction CSSs, and a good-re-centering capability at SLD, comparable to the capability of the low-friction CSSs, thus is able to combine effectively the inherent advantages of low-friction and high-friction CSS systems.

2) The initial gap of the gap damper is a key parameter for the fulfillment of the performance requirement at SLC, i.e. limiting the displacement demand for extreme earthquakes. Indeed, for low values of the initial gap (GF_1, GF_2), the gap damper is likely to be engaged during small vibrations before the occurrence of the peak displacement, leading to damage accumulation and increase of the initial gap, or threshold displacement, which will limit the energy absorbed by the gap damper in the cycle corresponding to the maximum displacement. Instead, the engagement of the gap damper for large displacements only (GF_3) mitigates the negative effects of the cumulative damage during minor amplitude cycles, and low-friction CSS with gap dampers having gap factor GF_3 provide ratios $d_{\max} / d_{\max}^{\mathrm{HF}}$ very close to unity (1.00, 1.03 and 1.04 for the three effective radii of curvature considered in the study, respectively). For this reason, the choice of GF_3 is recommended for hysteretic gap dampers with cumulative damage.

3) Without cumulative damage of the gap damper, the influence of the gap damper factor GF on the displacement demand at SLC becomes negligible. This is reasonable since the threshold displacement remains constant throughout the time-history response, irrespective of the

assumed initial gap d_{gap}.

4) The gap damper does not impair the good re-centering capability of low-friction CSSs at SLC and SLD. In particular, at SLC the residual displacement can even be lower (especially for R_1 and R_2) than the value $d_{\text{res}}^{\text{LF}}$. At SLD, the influence of the gap damper is totally negligible, and the performance of all the combinations of low-friction CSS + gap damper is comparable in terms of residual displacement to the one of the low-friction CSS alone. This occurs because the gap damper is not engaged for low-to-moderate seismic intensity levels typical of SLD earthquakes. However, this result has the merit of confirming that in the proposed realization scheme (Figure 3) the gap damper is able to provide supplemental energy dissipation to the isolation system without impairing its re-centering capability, and thus outperforms high-friction CSS systems or combination with supplemental energy dissipation devices that do not have a phased behavior, like e.g., fluid viscous dampers.

5) With regard to the maximum absolute acceleration, it must be noted that the engagement of the gap damper produces an increase of the acceleration response, as already reported in earlier studies from the literature [32]. In this regard, different observations can be made depending on the limit state. Indeed, the acceleration response is important especially for frequent earthquakes typical of SLD, where the protection of non-structural components is an important objective, whereas at SLC a collapse prevention performance level should be guaranteed. The increase of the acceleration response at SLC is unavoidable because it is inherent to the engagement of the gap damper, which ensures the aforementioned reduction of the displacement demand. On the other hand, assuming a gap damper factor GF_2 or GF_3 makes it possible to prevent the engagement of the gap damper for SLD earthquakes, thus providing a favorable low-level acceleration response in line with the one of the low-friction CSS. As a result, it is believed that the response in terms of acceleration for frequent earthquakes is not a major concern for the proposed isolation system, provided a sufficiently

large initial gap (at least 50% of the reduced displacement demand at SLC) is assumed in the design.

6) Some of the advantages of the proposed isolation system discussed above are valid for the low-friction CSS + gap damper, but are less significant for the medium-friction CSS + gap damper, as can be seen from the histograms. In particular, while a higher friction coefficient (medium-friction f_2 in place of low-friction f_1) results in a smaller displacement demand at SLC, the advantages in terms of re-centering capability and low acceleration response at SLD, typical of low-friction CSS systems, disappear. For this reason, in the authors' opinion it is recommended to combine gap dampers with low-friction CSSs so as to satisfactorily and simultaneously meet the performance requirements at both SLC and SLD.

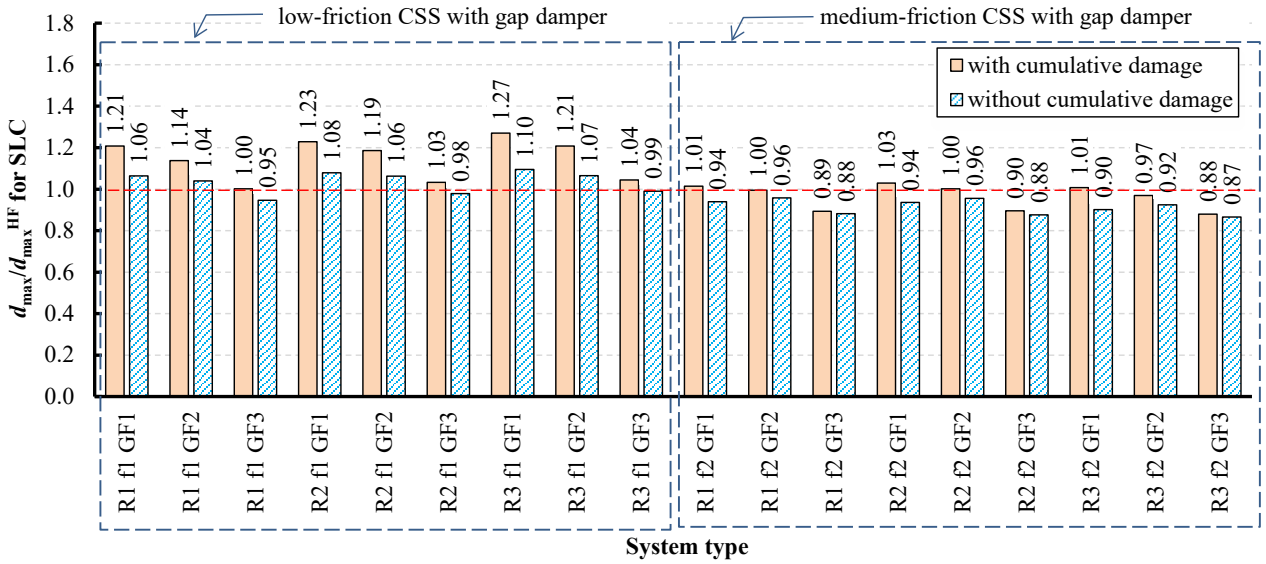

Figure 13 Seismic performance in terms of maximum displacement demand of combined CSS with gap damper compared to high-friction CSS system at SLC

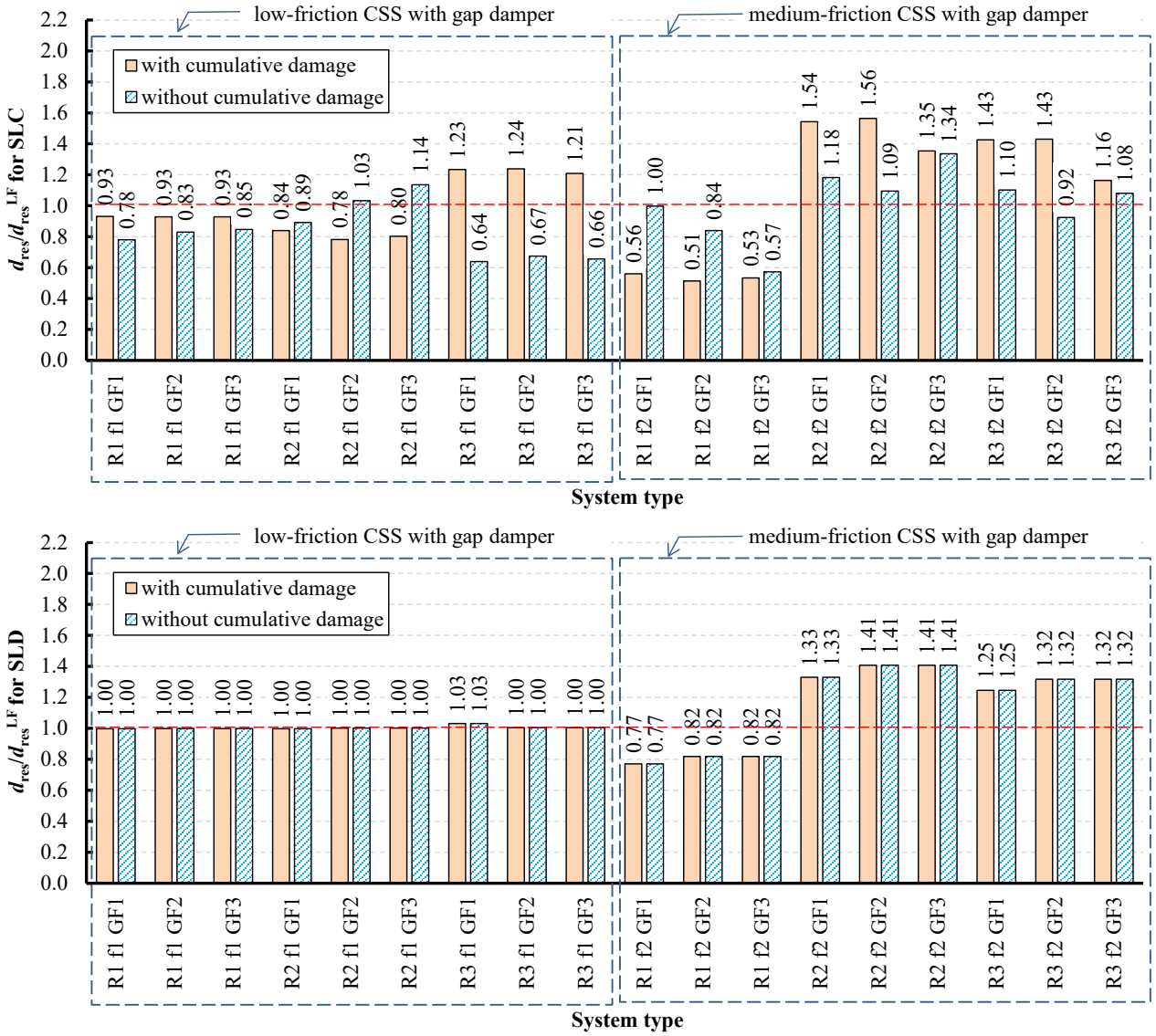

Figure 14 Seismic performance in terms of residual displacement of combined CSS with gap damper compared to low-friction CSS system at SLC (top) and SLD (bottom)

Strictly speaking, looking at the realization scheme in Figure 3, some impacts could occur at every engagement of the gap damper, thus affecting the behavior of the superstructure and involving higher-order modes (here neglected owing to the SDOF simplifying modeling assumption). These unavoidable impacts would be beneficial, since they entail an additional energy dissipation contribution, but also they somewhat modify the response compared to the one obtained in this paper. Consequently, the seismic performance indices (especially the absolute acceleration response) could be slightly different from that shown in Figure 12-Figure 15.

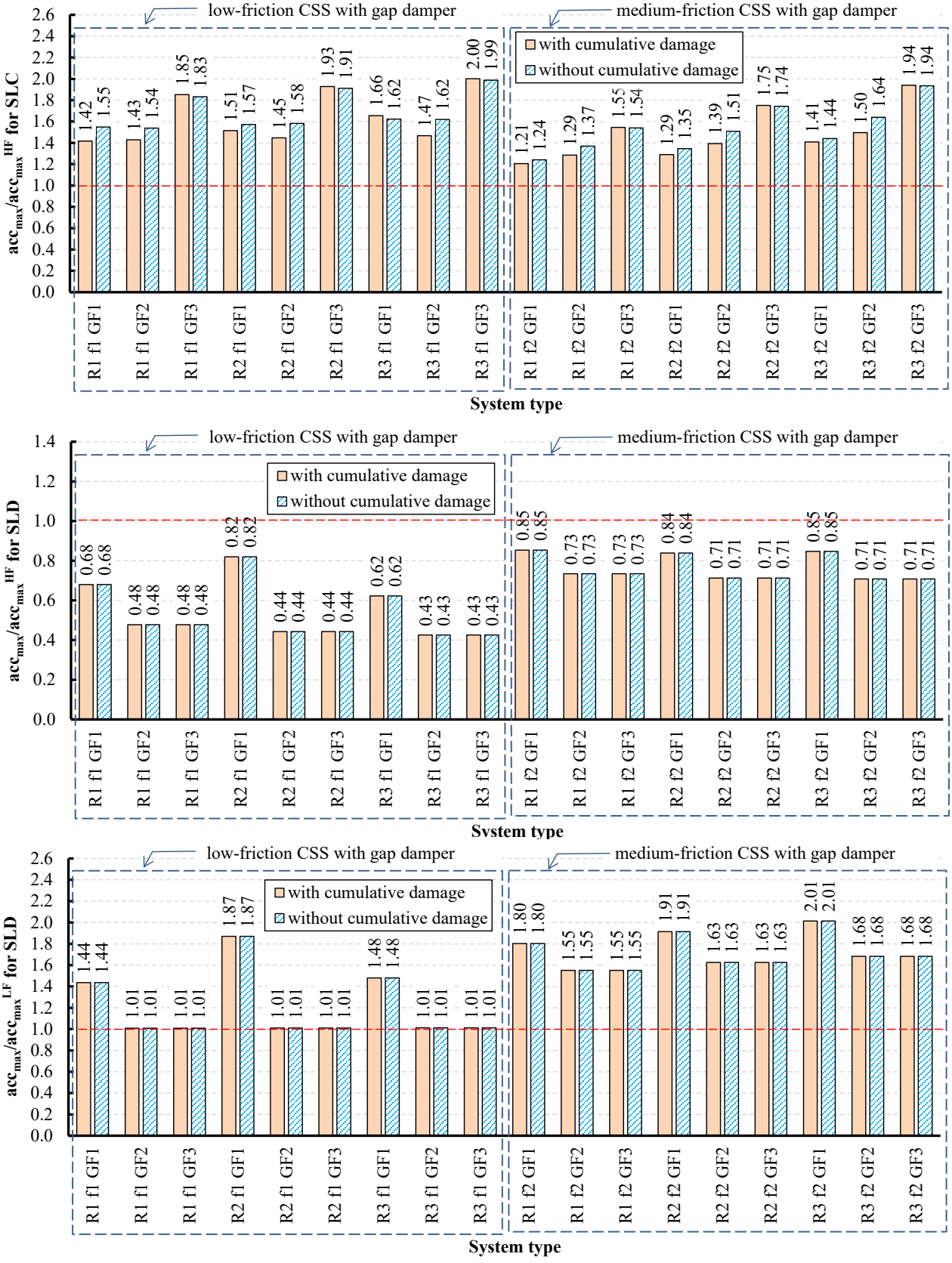

Figure 15 Seismic performance in terms of maximum absolute acceleration of combined CSS with gap damper compared to high-friction CSS system at SLC (top) and both high-friction and low-friction CSS at SLD (bottom)

5. CASE STUDY STRUCTURE

In this section, the seismic performance of the isolation system made of CSS combined with gap dampers is numerically assessed by considering a case study structure previously analyzed by the authors from an experimental point of view [30]. Shake-table tests were carried out at the University "Federico II" of Naples, Italy, on a 1:3 scale one-story steel frame with rectangular plan. The frame is isolated with four CSSs placed at the corners, as illustrated in Figure 16.

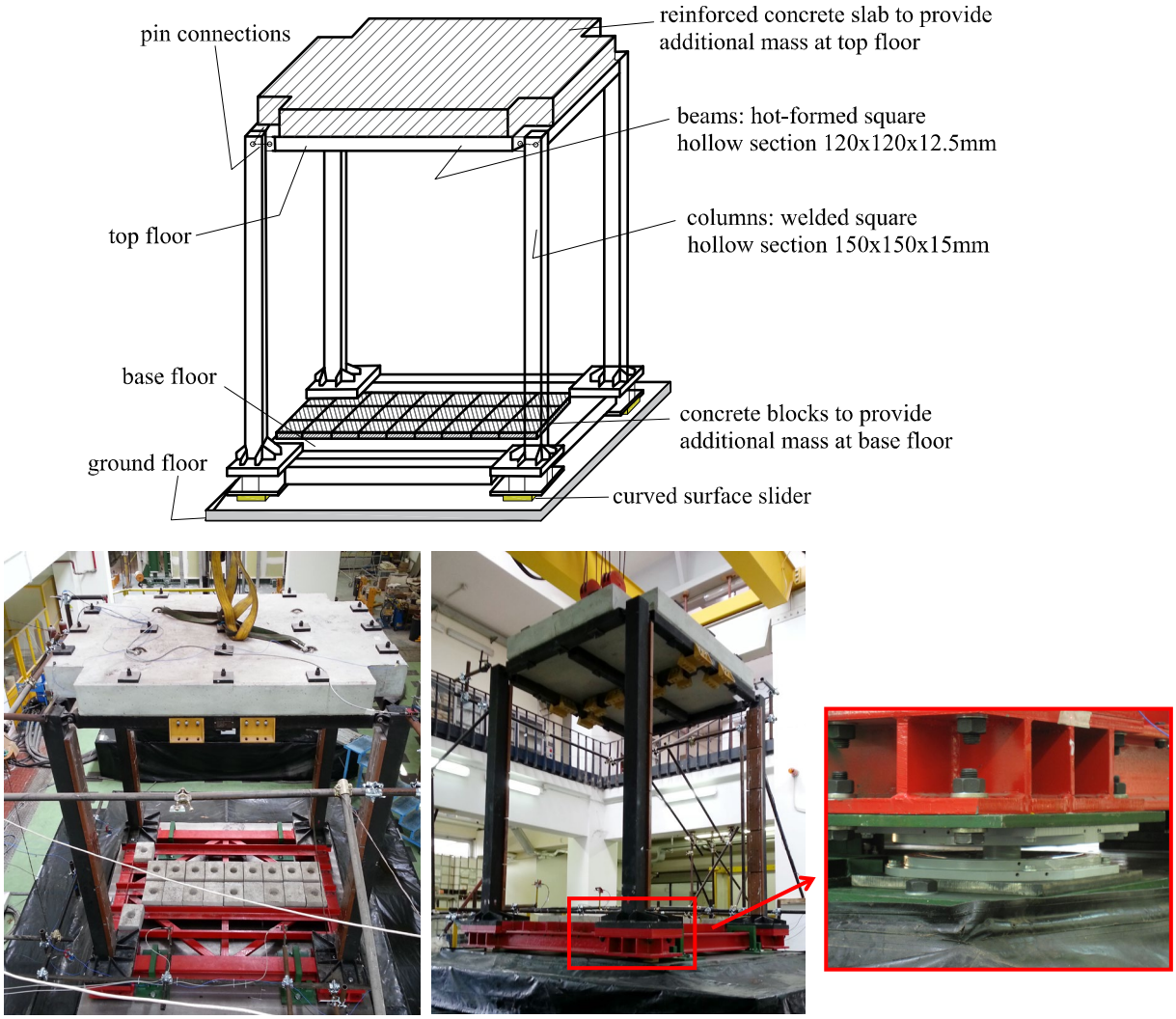

Figure 16 Shake table tests carried out on a 1:3 scale one-story steel frame isolated with curved surface sliders having different frictional characteristics

The steel frame has a rectangular plan of $2.65 \times 2.15\,\mathrm{m}$ and a total height of $2.90\,\mathrm{m}$, which are representative dimensions for an ordinary building at a 1:3 length scale. Details of testing equipment, prototype frame building and scale factors are given in [30]. A reinforced concrete slab (with

dimensions of $2.1 \times 2.65 \times 0.25\,\text{m}$) was placed on the top floor and 40 additional concrete blocks (each one with dimensions of $150 \times 235 \times 305\,\text{mm}$) were placed on the base floor, in order to provide a total mass equal to 8.2 ton. In particular, the base floor had a total mass equal to 3.26 ton, while the top floor had a total mass of 4.94 ton. Due to the symmetry of the structure, each of the four CSSs carried 1/4 of the total weight. The fundamental period of the fixed-base structure is 0.4 s.

Two different frictional characteristics of the sliding pads were considered in the experimental campaign and are numerically analyzed in this paper: 1) unfilled PTFE lubricated with silicon grease, referred to as low-friction (LF) material; 2) a not-lubricated PTFE-bronze composite, referred to as high-friction (HF) material. The isolators adopted in the experimental campaign were either double curved surface sliders (DCSSs) for LF pads, with an effective radius of curvature of 1485 mm and a displacement capacity of 260 mm, or single curved surface sliders (SCSSs) for HF pads, with an effective radius of curvature of 1500 mm and a displacement capacity of 165 mm [30].

The steel frame is modelled in OpenSees v. 2.5.4 [47], adopting 3D beam elements with consistent cross-sectional characteristics for columns and beams. The hysteretic behavior of the CSSs is reproduced by means of "*Single Friction Pendulum Bearing"* elements with an associated "*Velocity Dependent Friction*" law defined by Eq. (5) [48]. Small-scale tests performed on a custom biaxial testing equipment at the laboratory of Politecnico di Milano, Italy [35] are used to determine the parameters of the friction model for the two sliding materials, and the relevant friction vs. velocity curves are illustrated in Figure 17. The contact pressure used for the small-scale tests is the same as that experienced by the bearings in the shake-table tests, namely 7.10 MPa for LF pads, and 3.98 MPa for HF pads.

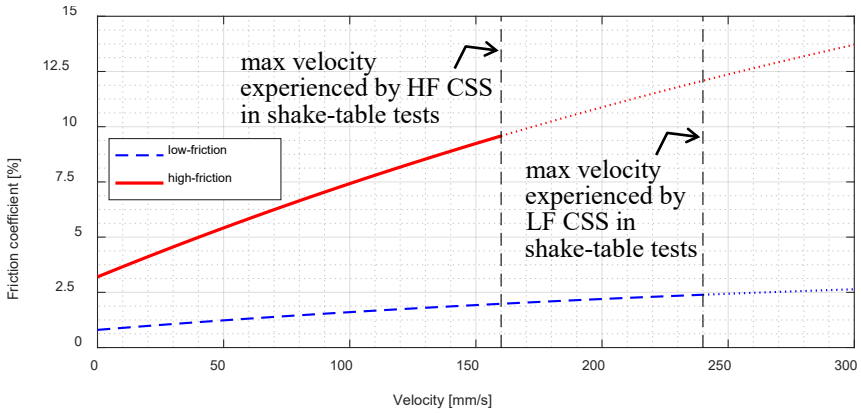

Figure 17 Velocity-dependent friction law of the two sliding pads adopted in the shake-table tests obtained through the experimental procedure described in [35]

Among the events selected for the shake-table tests in the experimental campaign [30], a sequence of three repeated identical ground motions corresponding to the Campano Lucano (CAT) earthquake, ID 287ya, station ST93, scaled to a PGA of 2.55 m/s^2 (SF equal to 1.43) is here considered in the finite element model. The peak ground velocity of this ground motion record is 43.90 cm/s, the kinematic pulse index (calculated as per Quaglini et al. [31]) is equal to 0.70 and the pulse period is equal to 1.58 s. Therefore, this record can be classified as a pulse-like event with pronounced directivity effect. Evidently, three identical repetitions of the same seismic input are very unlikely to occur in practice, while more realistic recorded mainshock and aftershock sequences were previously analyzed [31]. This specific sequence has been chosen here as an extreme case, because a remarkably different behavior between LF and HF CSS isolation system was experimentally observed in terms of displacement demand and re-centering capability. Moreover, this sequence highlighted the importance of residual displacements in view of possible accrual of displacements in case of aftershocks.

The displacement response of the LF and HF CSS isolation systems to the sequence of three repeated ground motion records is reported in Figure 18. An excellent agreement between experimental data and numerical results is noticed in terms of both peak displacement and residual displacement at the end of each shake, which confirms that the parameters adopted in the velocity-dependent friction model are consistent with the frictional characteristics of the sliding pads used in

the shake-table tests.

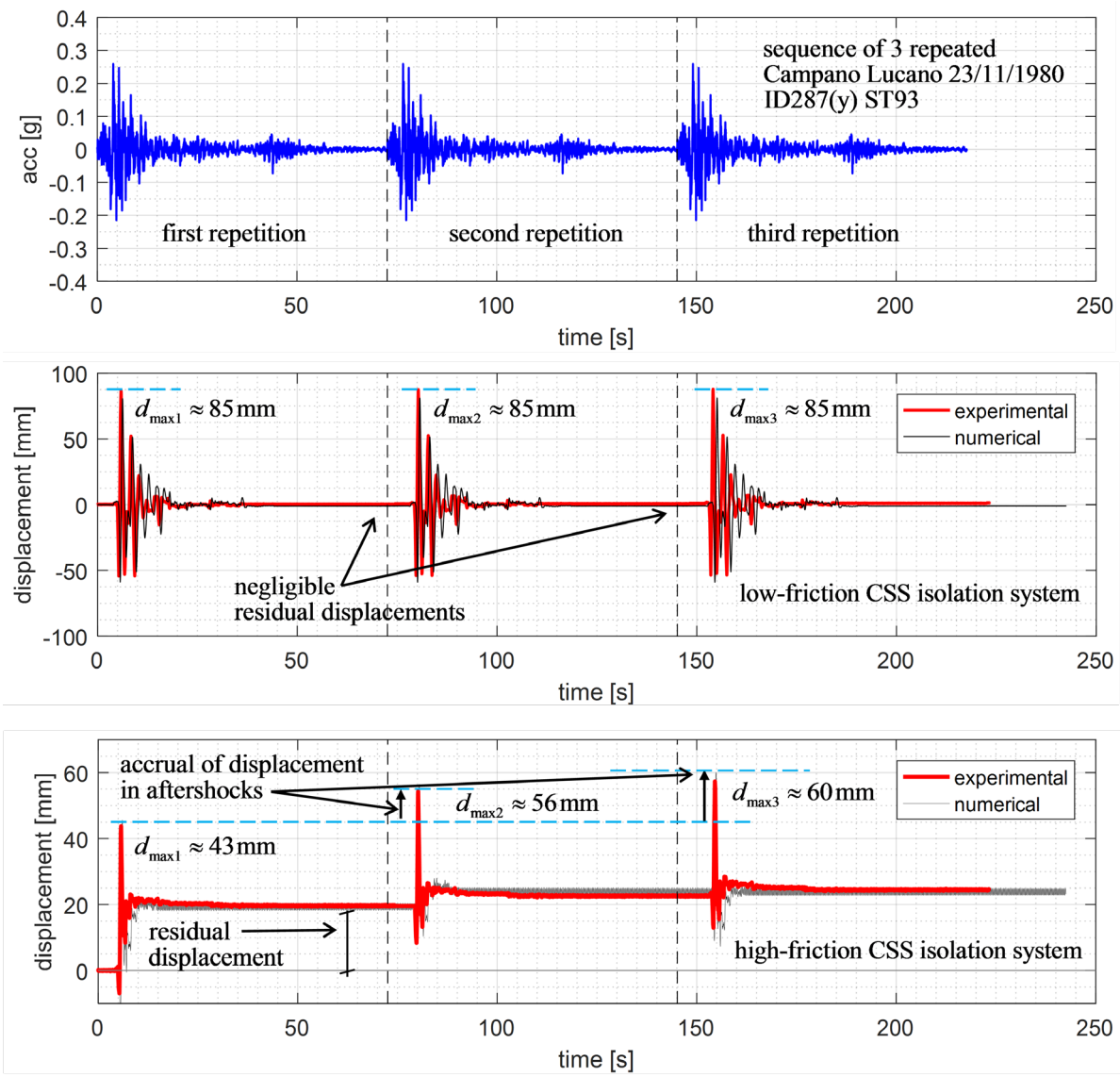

Figure 18 Experimental versus numerical response to a sequence of 3 repetitions of the Campano Lucano earthquake: acceleration time history (top), displacement response of low-friction CSS isolation systems (middle) and displacement response of high-friction CSS isolation system (bottom)

A considerably different behavior between the low-friction and the high-friction CSS isolation systems is observed. The high friction coefficient significantly reduces the displacement demand of the isolated structure (from 85mm to 43mm at the first shake) through the mechanism of energy dissipation, but the poor re-centering behavior of the HF CSS produces an accrual of residual displacement over the sequence of repetitions of the ground motion, whereas negligible residual displacements are observed with the LF CSS. In particular, the first shake induces a residual

displacement of the structure with HF CSSs, which is nearly half of the peak displacement (about 20mm). This residual displacement thus represents an initial offset of the isolation system during the second run of the ground motion, and contributes to increasing the peak displacement in the subsequent repetitions (up to 60mm at the third shake).

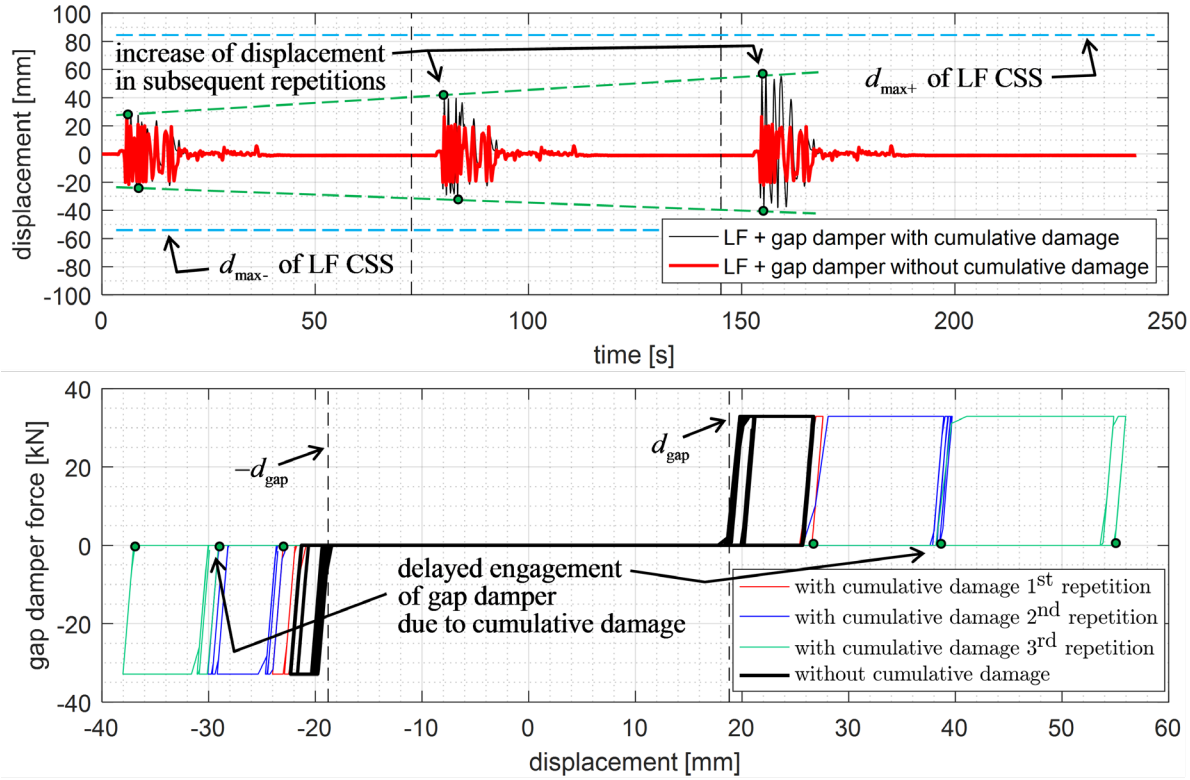

Figure 19 Response of combined isolation system to a sequence of 3 repetitions of the Campano Lucano earthquake: displacement response (top), and corresponding force-displacement loops of gap damper (bottom)

The same seismic input of the shaking table tests (three repetitions of the Campano Lucano earthquake) has been applied numerically to the case-study structure in which, in place of the traditional CSS isolation system, the proposed isolation system (low-friction CSSs + gap dampers) is implemented. In Figure 19, the response of the combined isolation layout (LF CSS + gap damper) is shown. The gap damper is designed according to the energy-based design procedure described in subsection 3.3. Motivated by the results of the parametric study, a gap factor GF_3 is chosen. The reduction factor RF is calculated assuming a target maximum displacement of 25mm, in order to assess the ability of the proposed isolation system to reduce the displacement demand even below the level of the HF CSS isolation system. The displacement demand of the LF CSS isolation system

without gap damper is also reported in the Figure as two dashed blue lines (positive and negative values) for comparative purposes. The gap damper is effective in reducing the displacement demand to the target level (maximum displacement of 26mm) at the first run of the sequence. For the second and third repetitions of the ground motion, different considerations can be made depending on the cumulative damage. Disregarding the cumulative damage leads to the same response during the three repetitions, because the force-displacement loops of the gap damper are simply replicated three times in an identical manner. In contrast, when the cumulative damage of the gap damper is taken into account, the peak displacement increases during the second and the third repetitions of the ground motion compared to the first shake due to the increase of the initial gap d_{gap}, and hence the delayed engagement of the gap damper, caused by accumulated plastic deformation. This drawback is inherently related to the use of conventional hysteretic steel dampers, viscous dampers or friction dampers that exhibit permanent deformation after being engaged in compression. However, the cumulative damage effect might be mitigated by using shape memory alloys that do not suffer from permanent deformation in place of classical steel elements for the hysteretic dampers, or introducing a re-centering mechanism to restore the initial position of the gap damper after being engaged. Notwithstanding, after three repetitions the maximum displacement attained by the proposed isolation system with cumulative damage is 55mm, which is lower than the maximum displacement attained by the LF CSS system (85mm) as well as by the HF CSS system (60mm), the latter being indeed affected by the accrual of displacement induced by its poor re-centering behavior.

6. CONCLUSIONS

An effective base-isolation system that combines low-friction CSS with hysteretic gap dampers was presented. The gap damper provides supplemental energy dissipation only when the isolation system exceeds a threshold displacement or initial gap while not being engaged otherwise.

The main findings of this research work can be summarized as follows:

1) The phased behavior of the gap damper realization scheme (Figure 3) developed in this paper does not impair the re-centering capability of the isolation system, since it is composed by two "compression-only" hysteretic elements that do not provide any reaction force during the coda stage of the ground motion or during free vibration of the isolation system in the neighborhood of its undeformed configuration.
2) A performance-oriented design procedure for the selection of the mechanical parameters of the hysteretic gap damper was developed in order to achieve a target maximum displacement during extreme events. As an example, the target displacement demand can be designed to be at the same level as (or even lower than) the one provided by an isolation system with high-friction CSSs.
3) The design procedure was numerically validated through nonlinear response history analyses in a parametric study including two intensities of the earthquake excitation (associated with two distinct performance requirements, namely no collapse requirements and serviceability requirements) and different CSS characteristics. The results of the parametric study demonstrate that the use of gap dampers avoids undesirable effects associated with high-friction CSS at the serviceability design earthquake, such as residual displacements and large structural accelerations, and is beneficial for reducing the displacement demand of low-friction CSS isolation systems during extreme earthquakes.
4) An issue of the proposed gap damper layout is the cumulative damage induced by accumulated plastic deformation, which can negatively affect the performance of the gap damper in terms of displacement reduction. However, assuming at the design stage an initial gap d_{gap} equal to 0.75 times the maximum expected displacement (gap factor GF_3) was found to be a viable choice to avoid or limit the cumulative damage. Smaller values of initial gap (GF_1, GF_2), corresponding to 1/4 and 1/2 times the maximum expected displacement, may emphasize the negative effects of cumulative damage, which lead to a delayed engagement of the gap

damper and, consequently, reduce its effectiveness in the displacement mitigation during extreme earthquakes. Without cumulative damage of the gap damper, the influence of the gap damper factor GF on the displacement demand during extreme earthquakes becomes negligible.

5) The engagement of the gap damper produces an increase of the acceleration induced in the isolated superstructure. In these regards, assuming a larger initial gap (GF_3) is also beneficial for serviceability requirements, since it prevents the engagement of the gap damper during low-intensity earthquakes, thus avoiding the increase of the structural acceleration during frequent earthquakes when the protection of non-structural components is an important objective. For serviceability earthquakes, the acceleration response of the proposed system with gap dampers and GF_3 is in line with that of low-friction CSSs without gap damper and, consequently, much lower than that of high-friction CSSs.

6) In order to show the effects of the poor re-centering capability of high-friction CSSs in promoting the displacement accrual, experimental results recorded during shake table testing of a one-third scale base-isolated steel frame building were presented. The same seismic input (a sequence of three repetitions of an accelerogram with pronounced directivity effect) was applied numerically to the case-study structure in which, in place of the traditional CSS isolation system, the proposed isolation system (low-friction CSSs + gap dampers) was implemented. The numerical results highlighted the excellent performance in terms of both reduction of seismic displacement (to a level even lower than the displacement observed with high-friction CSSs) and negligible residual displacement.

In conclusion, the proposed solution for base isolated structures is characterized by satisfactory energy dissipation alongside good re-centering capability, thus combining effectively and simultaneously the inherent advantages of low-friction and high-friction CSSs. Gap dampers introduce supplemental energy dissipation without negatively affecting the re-centering behavior,

thus outperforming alternative high-friction CSS systems or combinations with supplemental energy dissipation devices that do not have a phased behavior. Consequently, the proposed system (low-friction CSSs + gap dampers) outperforms both the high-friction CSS system, which suffers from a low re-centering capability, and the low-friction CSS system, which suffers from large displacement demand.

The work aims at representing a feasibility study for the proposed gap damper system in combination with CSS, which also justifies the use of simple unidirectional seismic excitations for the numerical analyses. Extension to in-plane bidirectional seismic excitations will be discussed in a future development of this research work. Moreover, before practical implementation of the system, elimination or at least mitigation of the cumulative damage effects inherent to hysteretic dampers realized with conventional steel elements would be necessary. The authors recognize two possible strategies: *i*) introducing a properly designed re-centering mechanism for the compression-only hysteretic elements, thus restoring the initial position of the gap damper after being engaged and reproducing the behavior of the idealized system "without cumulative damage" simulated in this paper; *ii*) keeping the realization scheme adopted in this paper (Figure 3) but using hysteretic elements that exploit the superelastic effects given by shape memory alloys, which do not suffer from residual permanent deformation. The development of a novel shape memory alloy gap damper is indeed the object of an ongoing research.

References

[1] Martelli A, Clemente P, De Stefano A, Forni M, Salvatori A, Recent development and application of seismic isolation and energy dissipation and conditions for their correct use, in Perspectives on European Earthquake Engineering and Seismology, (Ed: A. Ansal) Vol. 1, Springer, New York, USA 2014, 449.

[2] Saitta F, Clemente P, Buffarini G, Bongiovanni G. Seismic analysis and retrofit of a mid-rise building. In: Papadrakakis M, Papadopoulos V, Plevris V, editors. Proceedings of COMPDYN 2015. Crete Islands, Greece; 25–27 May 2015. p. 3909–18.

[3] Caliò I, Marletta M, Vinciprova F. Seismic response of multi-storey buildings base-isolated by friction devices with restoring properties. Comput Struct 2003;81:2589–99.

[4] Castaldo P, Palazzo B, Della Vecchia P. Seismic reliability of base-isolated structures with friction pendulum bearings. Eng Struct 2015;95:80–93.

[5] Nagarajaiah, S., & Xiaohong, S. (2000). Response of base-isolated USC hospital building in Northridge earthquake. Journal of Structural Engineering, 126(10), 1177-1186.
[6] Naeim F, Kelly JM. Design of Seismic Isolated Structures: From Theory to Practice. John Wiley & Sons. New York, 1999.
[7] Zayas V, Low S, Mahin S, The FPS earthquake resisting system. Report No. CB/EERC-87/01, Earthquake Engineering Research Center, University of California, Berkeley, 1987.
[8] Maurer SE webpage: https://www.maurer.eu/.
[9] FIP Industriale web page: https://www._pindustriale.it/.
[10] Mageba webpage: https://www.mageba.ch/en/.
[11] Anagnostopoulos SA, Spiliopoulos KV. An investigation of earthquake induced pounding between adjacent buildings. Earthq Eng Struct Dyn 1992; 21:289-302.
[12] Clark PW, Aiken ID, Kelly JM. Experimental studies of the ultimate behavior of seismically-isolated structures. Earthquake Engineering Research Center, University of California, 1997.
[13] Panchal VR, Jangid RS. Seismic response of structures with variable friction pendulum system. Journal of Earthquake Engineering 2009; 13(2):193–216.
[14] Lu LY, Lee TY, Yeh SW. Theory and experimental study for sliding isolators with variable curvature. Earthquake Engineering and Structural Dynamics 2009; 40(14):1609–1627.
[15] Yang JN, Danielians A, Liu SC. Aseismic hybrid control systems for building structures. J Eng Mech 1991; 117: 836-853.
[16] Taniguchi T, Der Kiureghian A, Melkumyan M. Effect of tuned mass damper on displacement demand of base-isolated structures. Eng Struct 2008; 30:3478-3488.
[17] De Domenico D, Ricciardi G. Earthquake-resilient design of base isolated buildings with TMD at basement: Application to a case study. Soil Dyn Earth Eng 2018; 113: 503-521.
[18] De Domenico D, Ricciardi G. An enhanced base isolation system equipped with optimal Tuned Mass Damper Inerter (TMDI). Earthq Eng Struct Dyn 2018; 47: 1169-1192.
[19] De Domenico D, Deastra P, Ricciardi G, Sims ND, Wagg DJ. Novel fluid inerter based tuned mass dampers for optimised structural control of base-isolated buildings. Journal of the Franklin Institute 2019; 356(14): 7626-7649.
[20] De Domenico D, Ricciardi G. Optimal design and seismic performance of tuned mass damper inerter (TMDI) for structures with nonlinear base isolation systems. Earthquake Engineering & Structural Dynamics 2018; 47(12): 2539-2560.
[21] Hashimoto T, Fujita K, Tsuji M, Takewaki I. Innovative base-isolated building with large mass-ratio TMD at basement for greater earthquake resilience. Future Cities and Environment 2015; 1:9: 1-19.
[22] Peng Y, Ding L, Chen J, Villaverde R. Experimental study of sliding hydromagnetic isolators for seismic protection. Journal of Structural Engineering ASCE 2019; 145(5): 04019021.
[23] Peng Y, Ding L, Chen J. Performance evaluation of base-isolated structures with sliding hydromagnetic bearings. Structural Control and Health Monitoring 2019; 26(1): e2278.
[24] Peng Y, Huang T. Sliding implant-magnetic bearing for adaptive seismic mitigation of base-isolated structures. Structural Control and Health Monitoring 2019; 26(10): e2431.
[25] Kelly JM. The role of damping in seismic isolation. Earthq Eng Struct Dyn. 1999; 28:3-20.
[26] Medeot R. Re-centring capability evaluation of seismic isolation systems based on energy concepts. In Proceedings of the 13th world conference on earthquake engineering 2004; Vancouver, Canada, Paper Vol. 3106.
[27] Katsaras CP, Panagiotakos TB, Kolias B. Restoring capability of bilinear hysteretic seismic isolation systems. Earthquake Engineering & Structural Dynamics 2008; 37(4): 557-575.
[28] Cardone D, Gesualdi G, Brancato P. Restoring capability of friction pendulum seismic isolation systems. Bulletin of Earthquake Engineering 2015; 13(8): 2449-2480.
[29] Ponzo FC, Di Cesare A, Leccese G, Nigro D. Shake table testing on restoring capability of double concave friction pendulum seismic isolation systems. Earthquake Engineering & Structural Dynamics 2017; 46(14): 2337-2353.
[30] Quaglini V, Gandelli E, Dubini P. Experimental investigation of the re-centring capability of curved surface sliders. Structural Control and Health Monitoring 2017; 24(2): e1870.
[31] Quaglini V, Gandelli E, Dubini P, Limongelli MP. Total displacement of curved surface sliders under nonseismic and seismic actions: A parametric study. Structural Control and Health Monitoring 2017; 24(12): e2031.

[32] Zargar, H., Ryan, K. L., & Marshall, J. D. (2013). Feasibility study of a gap damper to control seismic isolator displacements in extreme earthquakes. Structural Control and Health Monitoring, 20(8), 1159-1175.
[33] Rawlinson TA, Marshall JD, Ryan KL, Zargar H. Development and experimental evaluation of a passive gap damper device to prevent pounding in base-isolated structures. Earthquake Engineering & Structural Dynamics 2015; 44(11): 1661-1675.
[34] Zargar H, Ryan KL, Rawlinson TA, Marshall JD. Evaluation of a passive gap damper to control displacements in a shaking test of a seismically isolated three-story frame. Earthquake Engineering & Structural Dynamics 2017; 46(1): 51-71.
[35] Quaglini V, Dubini P, Poggi C. Experimental assessment of sliding materials for seismic isolation systems. Bull Earthq Eng 2012; 10: 717–740.
[36] Dolce M, Cardone D, Croatto F. Frictional behaviour of steel-PTFE interfaces for seismic isolation. Bull Earthq Eng 2005; 3(1): 75-99
[37] CEN Eurocode 8: design of structures for earthquake resistance—Part 1: General rules, seismic actions and rules for buildings, EN1998-1:2004. European Committee for Standardization, Bruxelles, Belgium, 2004.
[38] CEN Eurocode 8: design of structures for earthquake resistance—Part 2: Bridges, EN1998-2:2005 + A1:2011. European Committee for Standardization, Bruxelles, Belgium, 2005.
[39] Ismail M, Rodellar J, Pozo F. An isolation device for near-fault ground motions. Structural Control and Health Monitoring 2014; 21(3): 249–268.
[40] Lomiento G, Bonessio N, Benzoni G. Friction model for sliding bearings under seismic excitation. J. Earthq. Eng. 2013; 17: 1162–1191.
[41] Quaglini V, Bocciarelli M, Gandelli E, Dubini P. Numerical assessment of frictional heating in sliding bearings for seismic isolation. Journal of Earthquake Engineering 2014; 18(8): 1198-1216.
[42] De Domenico D, Ricciardi G, Benzoni G. Analytical and finite element investigation on the thermo-mechanical coupled response of friction isolators under bidirectional excitation. Soil Dyn Earthq Eng 2018; 106:131-147.
[43] Quaglini V, Gandelli E, Dubini P. Numerical investigation of curved surface sliders under bidirectional orbits. Ingegneria Sismica - International Journal of Earthquake Engineering 2019 (2).
[44] Constantinou M, Mokha A, Reinhorn AR. Teflon bearings in base isolation II: modeling. J Struct Eng 1990;116(2):455–74.
[45] Vayas I INNOSEIS Project - Valorization of INNOvative anti-SEISmic devices. 2017. Deliverables available at: http://innoseis.ntua.gr/deliverables.php?deliverable=reports
[46] De Domenico D, Ricciardi G, Takewaki I. Design strategies of viscous dampers for seismic protection of building structures: a review. Soil Dynamics and Earthquake Engineering 2019; 118: 144-165.
[47] McKenna F, Fenves GL, Scott MH, Jeremic B. Open System for Earthquake Engineering Simulation (OpenSees), Pacific Earthquake Engineering Research Center (PEER), Berkeley, USA 2000.
[48] OpenSeesWiki, online manual, available at: http://opensees.berkeley.edu/wiki/index.php/Main_Page.
[49] NTC2018. CSLLPP - Consiglio Superiore dei Lavori Pubblici. Norme Tecniche per le Costruzioni. Gazzetta Ufficiale 495 della Repubblica Italiana, No. 42 of 20 February 2018. Rome, Italy, (in Italian).
[50] Iervolino I, Galasso C, Cosenza E. REXEL: computer aided record selection for code-based seismic structural analysis. Bulletin of Earthquake Engineering 2010; 8: 339-362.
[51] Ambraseys N, Smit P, Sigbjornsson R, Suhadolc P Margaris B. Internet-Site for European Strong-Motion Data, European Commission, Research-Directorate General, Environment and Climate Programme 2002.
[52] Gandelli E, Quaglini V, Dubini P, Limongelli MP, Capolongo S. Seismic isolation retrofit of hospital buildings with focus on non-structural components, Ingegneria Sismica - International Journal of Earthquake Engineering 2018; Vol. 2018 (4).
[53] Gandelli E, Taras A, Distl J, Quaglini V. Seismic retrofit of hospitals by means of hysteretic braces: influence on acceleration-sensitive non-structural components. Frontiers in Built Environment – Earthquake Engineering 2019; doi: 10.3389/fbuil.2019.00100.